Hedgehog signaling acts as cell fate determinant during adult tissue repair

Alessandra M. Norris[1], Connor D. Johnson[1], Lylybell Y. Zhou[1], Ambili Appu[1], David W. McKellar[2], Benjamin D. Cosgrove[2] and Daniel Kopinke[1*].

[1] Department of Pharmacology and Therapeutics, Myology Institute, University of Florida, Gainesville, FL, USA.

[2]Meinig School of Biomedical Engineering, Cornell University, Ithaca, NY, USA

[*]Correspondance: dkopinke@ufl.edu

Abstract

Failed tissue regeneration often results in fatty fibrosis, the replacement of healthy cells with fibrotic scar and fat tissue. However, the causative signals remain largely unknown. Here, we describe how the Hedgehog (Hh) signaling pathway controls the fate of fibro/adipogenic progenitors (FAPs), the cellular origin of fatty fibrosis. Using conditional mutagenesis and pharmacological Hh modulators, we identify DHH as the main ligand through which Hh restricts intramuscular fat (IMAT) formation and promotes muscle regeneration. In contrast, conditionally activating Hh specifically in FAPs skews them from an adipogenic towards a fibrogenic fate resulting in massive fibrotic scar tissue. Surprisingly, FAP-specific Hh activation also impairs myoblast differentiation leading to muscle regeneration defects. Together, our data reveal novel post-developmental functions of Hh signaling in balancing tissue regeneration and fatty fibrosis. Moreover, they provide the exciting possibility that mis-regulation of the Hh pathway with age and disease could be a major driver of pathological IMAT formation, thereby representing an attractive therapeutic target.

Introduction

Coordinating intercellular signaling between adult stem cells and their niche to balance differentiation and self-renewal is critical for regenerating complex tissues after injury. Successful regeneration of skeletal muscle depends on the interplay of two distinct stem/progenitor cell populations: dedicated muscle stem cells (MuSCs) and fibro/adipogenic progenitors (FAPs). MuSCs differentiate into myoblasts and either fuse together to form new muscle fibers or fuse with existing fibers to repair damaged ones [1, 2, 3, 4]. FAPs are a multipotent mesenchymal stem/stromal cell population present in most adult organs including skeletal muscle [5, 6]. FAPs build and maintain the extracellular matrix and are crucial during the repair of damaged tissues by secreting beneficial factors [7, 8, 9, 10, 11, 12, 13, 14, 15]. With age and disease, FAPs can also differentiate into myofibroblasts, the cellular origin of tissue fibrosis [7, 15], and adipocytes, which will form intramuscular fat (IMAT) [7, 8, 14, 15, 16, 17, 18, 19]. The infiltration and replacement of healthy muscle tissue with IMAT and scar tissue, also called fatty fibrosis, is a prominent feature of Duchenne Muscular Dystrophy (DMD) and other neuromuscular diseases, as well as sarcopenia, obesity, and diabetes [18, 20, 21, 22, 23, 24, 25, 26, 27, 28, 29]. It remains unclear what signal(s) balance the beneficial functions and multiple fates of FAPs.

Through screens to identify factors that might control FAPs, we recently reported that FAPs are the main ciliated cell type in muscle that can sense and transduce Hedgehog (Hh) signaling [8]. Primary cilia are small cellular antennae that receive and interpret extracellular cues including the Hh pathway [30, 31]. Hh is a long-range signaling pathway that is activated through secreted ligands such as Sonic (SHH), Indian (IHH) or Desert (DHH) Hedgehog. Uniquely, vertebrate Hh signaling fully relies on the primary

cilium for its function [30, 31]. In the absence of Hh ligands, the cilium processes the GLI (glioma-associated oncogene homolog) transcription factors into their repressor form to maintain repression of Hh target genes [30, 31]. Upon binding of a ligand to the Hh receptor Patched1 (Ptch1), a negative regulator of the pathway, Smoothened (Smo) accumulates in the cilium to activate the GLIs [30, 31]. As a consequence of this intimate relationship between cilia and Hh, only ciliated cells can respond to Hh ligands.

During skeletal muscle development, Hh signaling helps to initiate the myogenic program [32, 33, 34]. In mature muscle, while the Hh pathway only displays low activity under homeostatic conditions, acute injuries robustly activate Hh signaling [8, 35, 36, 37, 38]. In contrast, Hh activity is severely blunted with age and in *mdx* mice, a mouse model of DMD, as well as in a chronic injury model induced by glycerol [8, 35, 36, 37, 39]. Our recent work demonstrated that removal of FAP cilia resulted in Hh de-repression and subsequent Hh activation, albeit at low levels, due to loss of GLI3 repressor [8]. Once activated, we found that the Hh pathway potently inhibited the *in vivo* differentiation of FAPs into adipocytes via upregulation of the secreted anti-adipogenic factor TIMP3 (Tissue inhibitor of Metalloproteinases 3). At the same time, we also found that FAP-specific Hh activation promoted myofiber regeneration post injury and prevented the decline of muscle atrophy in a mouse model of DMD.

Thus, Hh can act as a potent anti-adipogenic [8, 40, 41, 42] and pro-myogenic [8, 40, 43, 44] signal once activated. However, its endogenous role, including the responsible ligand, during skeletal muscle regeneration remains unresolved. Here, we identify DHH as the main Hh ligand through which Hh balances muscle regeneration and IMAT formation. We find that Hh, via DHH, acts as an endogenous adipogenic brake by inducing TIMP3 and, once lost, results in increased IMAT formation after an acute injury. We also define the time window when Hh activity is required to impact adipogenesis and myogenesis. Surprisingly, we find that constitutive activation of Hh specifically within FAPs pushes FAPs away from an adipogenic towards a fibrogenic fate resulting in massive scar tissue formation and impaired myogenesis. Thus, DHH-induced Hh signaling, through cell autonomous and non-autonomous roles, balances IMAT formation and muscle regeneration pointing to ciliary Hh signaling as a novel therapeutic strategy to combat IMAT formation.

Results

<u>Acute muscle injury induces Hedgehog activation, via its ligand DHH, in FAPs and MuSCs.</u>

The identity of the endogenous Hh ligand required for muscle regeneration remained unknown with evidence suggesting both SHH [35, 36, 37] and DHH [38]. To objectively determine which Hh ligand(s) is/are expressed in muscle, we utilized single-cell gene expression analysis. We quarried unpublished and public single-cell RNAseq (scRNAseq) data sets of skeletal muscle at different time points pre- and post-acute muscle injury, as previously described [45], to ask which Hh ligand is expressed by which cell type (Fig 1a). Intriguingly, our data indicate that, *Shh* and *Ihh* are undetectable, while *Dhh* is potently expressed within endothelial and neural cell (mainly comprised of Schwann cells) populations (Fig 1b). These data confirm previous observations that Schwann cells within the peripheral nervous system [38, 46], as well as endothelial cells [47], are capable of expressing *Dhh*. Our data also demonstrate that *Dhh* is rapidly induced upon injury before returning to baseline levels by 10 days post injury (dpi) (Fig 1b). Asking which cells display an active Hh signature, we mined the dataset for cells expressing the GLI transcription factors *Gli1, 2 & 3*. We found that FAPs are the main cell population that display active Hh signaling followed by MuSCs (Fig 1c). As only ciliated cells can respond to Hh signaling, these results fit with our [8] and other previous findings [40, 43, 44, 48, 49] that FAPs and MuSCs are the only ciliated cell populations in muscle with FAPs making up the highest proportion of ciliated cells. Thus, our data reveal that an acute muscle injury activates Hh signaling within ciliated FAPs and MuSCs through induction of *Dhh* (Fig 1d). Interestingly, we have previously shown that Hh signaling is being repressed after an adipogenic injury, caused by GLY [8]. Given the fact that Hh is a potent anti-adipogenic signal in muscle [8, 40], these results also suggest that Hh activity levels could dictate how much IMAT is being allowed to form.

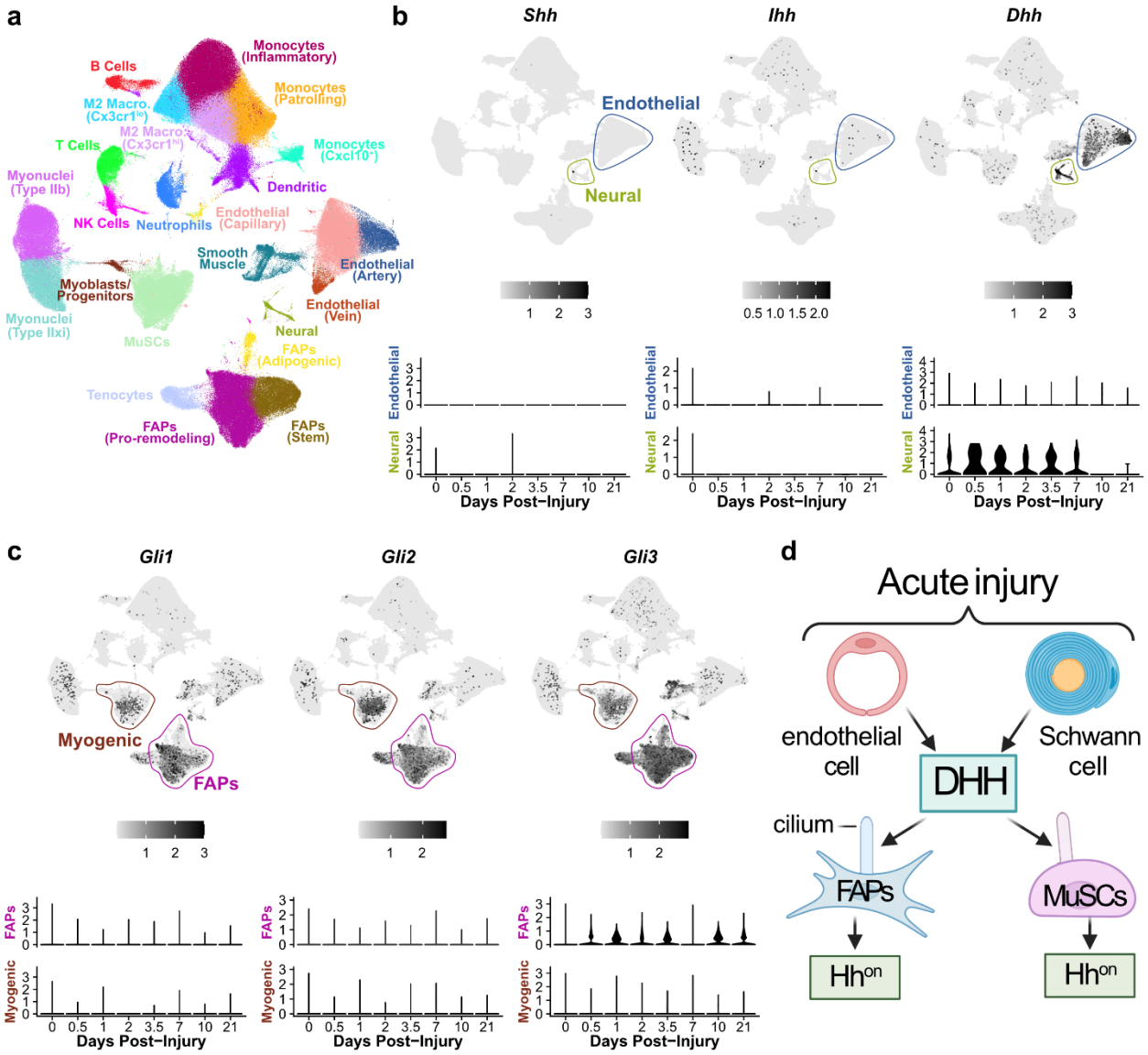

Figure 1. *Dhh* is the main Hh ligand being expressed after an acute injury and sensed by FAPs and MuSCs. **a)** UMAP plot of 111 published single-cell and single-nucleus RNA-sequencing datasets of skeletal muscle before and after injury. Identification and clustering of cell types was derived from Harmony batch correction (see *Materials & Methods*). **b)** Top: UMAP plots showing log-normalized expression of the Hh ligands *Shh, Ihh*, and *Dhh*. Bottom: Log-normalized expression for each ligand within the endothelial clusters (capillary, artery, and vein endothelial cells) or neural cluster at different time points post injury. **c)** Top: UMAP plots showing log-normalized expression of the Hh-controlled transcription factors *Gli1, Gli2* & *Gli3*. Bottom: Log-normalized expression for each *Gli* gene within the FAP (stem, pro-remodeling, and adipogenic) or myogenic (MuSCs and myoblasts) clusters at different time points post injury. **d)** *Model*: After an acute injury, endothelial and Schwann cells express *Dhh*. DHH is then sensed by ciliated FAPs and MuSCs leading to activated Hh signaling.

<u>Hedgehog signaling, via DHH, restricts IMAT formation</u>

To determine the endogenous function of DHH and the Hh pathway during muscle regeneration, we utilized a murine Dhh null mouse model (*Dhh*$^{-/-}$). *Dhh*$^{-/-}$ mice are viable, phenotypically normal and have a normal life span [38, 50]. Confirming and extending these reports, we find that uninjured 7-month-old *Dhh*$^{-/-}$ mice display no gross phenotypical abnormalities including no differences in total body weight, or uninjured Tibialis Anterior (TA) weight compared to littermate controls (*Dhh*$^{+/-}$ and *Dhh*$^{+/+}$) (Fig. S1a). As our previous data demonstrated that activating the Hh pathway potently blocks IMAT, we next determined if loss of DHH would result in increased IMAT formation. We selected cardiotoxin (CTX) as our injury

model since CTX induces Hh activity and causes little fat formation [8, 51, 52, 53]. RT-qPCR of whole muscle lysate 7 days post injury (dpi) confirmed complete loss of *Dhh* expression in *Dhh*$^{-/-}$ mice (Fig. S1b and c) resulting in decreased Hh activity as shown by expression for the two Hh downstream targets *Gli1* and *Ptch1* (Fig. 1b). To assess IMAT formation, we quantified the number of PERILIPIN^{+} adipocytes in uninjured or injured TAs from *Dhh*$^{-/-}$ and control mice. We found no difference in IMAT formation in uninjured TAs between control and *Dhh*$^{-/-}$ mice demonstrating that loss of *Dhh* does not cause ectopic IMAT in the absence of injury. In contrast, there was a significant increase in IMAT 21 days post CTX injury in *Dhh*$^{-/-}$ mice compared to controls (Fig 1c and d). This observation was independent of sex, and we did not detect any differences between *Dhh*$^{+/+}$ and *Dhh*$^{+/-}$ control animals (Fig. S1d). Acute muscle injuries result in transient fibrosis [11, 54]. As IMAT and fibrosis are highly correlated with disease progression [28, 55, 56], we next asked whether loss of *Dhh* also affected injury-induced fibrosis. To visualize the extracellular matrix (ECM), we stained control and *Dhh*$^{-/-}$ mice 21 days post CTX injury with picrosirius

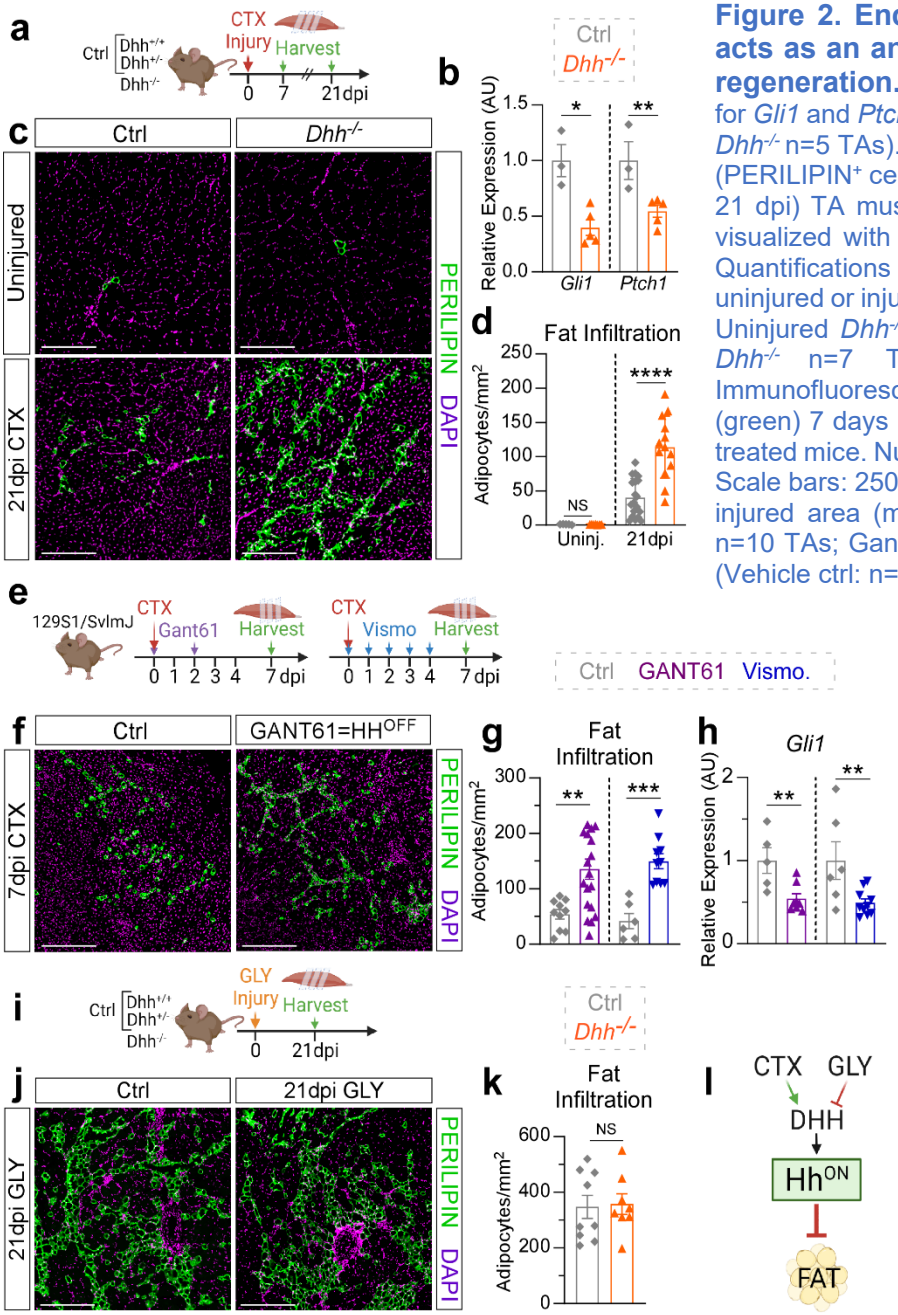

Figure 2. Endogenous Hh, activated by DHH, acts as an anti-adipogenic break during acute regeneration. a) Experimental outline. **b)** RT-qPCR for *Gli1* and *Ptch1* at 7dpi post CTX injury (ctrl n=3 TAs; *Dhh*$^{-/-}$ n=5 TAs). **c)** Immunofluorescence for adipocytes (PERILIPIN^{+} cells, green) in uninjured and injured (CTX 21 dpi) TA muscle of ctrl and *Dhh*$^{-/-}$ mice. Nuclei are visualized with DAPI (purple). Scale bar: 250 µm. **d)** Quantifications of the number of adipocytes per uninjured or injured area (mm^2) (Uninjured ctrl n=5 TAs, Uninjured *Dhh*$^{-/-}$ n=7 TAs; 21dpi ctrl n=13 TAs; 21dpi *Dhh*$^{-/-}$ n=7 TAs). **e)** Experimental outline. **f)** Immunofluorescence for PERILIPIN^{+} adipocytes (green) 7 days post CTX injury of vehicle and Gant61-treated mice. Nuclei were visualized with DAPI (purple). Scale bars: 250 µm. **g)** Quantification of adipocytes per injured area (mm^2) 7 dpi of Gant61 (vehicle treated: n=10 TAs; Gant61 treated: n= 18 TAs) or Vismodegib (Vehicle ctrl: n=6 TAs; Vismodegib treated: n=10 TAs) experimental mice. **h)** RT-qPCR for *Gli1* of Gant61 (Vehicle ctrl: n=5 TAs; Gant61 treated: n=7 TAs) and Vismodegib (vehicle ctrl: n=6 TAs; Vismodegib treated: n=10 TAs) experimental mice. **i)** Experimental outline. **j)** Immunofluorescence to visualize adipocytes (PERILIPIN^{+} cells, green) 21 days post GLY injury in ctrl and *Dhh*$^{-/-}$ mice. Scale bars: 250 µm. **k)** Quantification of adipocytes per injured area (mm^2) of ctrl (n=9 TAs) and Dhh$^{-/-}$ (n=8 TAs) mice 21 days post GLY injury. **l)** *Model:* CTX, but not GLY, activates the Hh pathway through induction of DHH. Once active, Hh represses IMAT formation. All data are represented as mean ± SEM. (b-d; g-h; k) An unpaired two-tailed t test was used. A p value less than 0.05 was considered statistically significant where: * p≤ 0.05, ** p≤ 0.01, *** p≤ 0.001 and **** p≤ 0.0001.

red, which identifies collagen fibers [11, 57]. The lack of difference in the amount of collagen deposition between genotypes, indicates that loss of Hh signaling has no effect on fibrosis (Fig. S1e). Together, these results demonstrate that DHH is the main Hh ligand that activates the Hh pathway to limit IMAT formation, but not fibrosis, during muscle regeneration.

To corroborate our findings, we utilized a pharmacological approach to acutely inhibit Hh activation at various time points post injury. The small molecule Gant61 is a selective inhibitor of Gli1- and Gli2-mediated transcription [58, 59], while Vismodegib is an FDA-approved selective inhibitor of Smo [60]. We injured TA muscles of wild type mice with CTX and administered Gant61 at 0 and 2 dpi, while a separate cohort was administered Vismodegib daily from 0-4 dpi (Fig. 2e). Successful inhibition of CTX-induced Hh activation after both Gant61 and Vismodegib treatment was determined by RT-qPCR for *Gli1* (Fig. 2h). As a result of repressed Hh signaling, treatment with Gant61 and Vismodegib allowed ectopic IMAT formation (Fig. 2f and g) similar to that observed after loss of DHH (Fig. 2c). These results confirm that acute induction of Hh signaling, via DHH, is required to limit IMAT formation during regeneration.

While an acute injury, for example caused by CTX or NTX (Fig 1b) [8], induces *Dhh*, and subsequent Hh activation, we have previously demonstrated that a highly adipogenic injury, induced by glycerol (GLY) injection [51, 52, 53, 61, 62], represses *Dhh* and Hh activity [8]. To determine if the increase of IMAT after a GLY-induced injury is due to repressed levels of *Dhh*, we next evaluated IMAT formation in *Dhh*$^{-/-}$ mice 21 days post GLY injury (Fig. 2l). As expected, we found that the number of PERILIPIN-expressing adipocytes was comparable between *Dhh*$^{-/-}$ and control mice. This indicates that a GLY injury suppress Hh activation allowing IMAT to form and that further reduction of Hh signaling via loss of *Dhh* has no additional impact on IMAT. Taken together, our data highlight that Hh signaling, via DHH, controls IMAT formation in skeletal muscle and that, depending on the type of injury, differential expression of *Dhh* and subsequent induction of the Hh pathway dictates how much IMAT is allowed to form.

<u>DHH is required and necessary for overall muscle regeneration</u>

We and others have shown that exogenous activation of the Hh pathway promotes muscle regeneration [8, 37, 40, 43]. To explore the role of DHH during myogenesis, we assessed myofiber regeneration 21 days post CTX injury in *Dhh*$^{-/-}$ and control mice (Fig. 3a). Myogenesis was assessed by measuring the cross-sectional area (CSA) of myofibers, a critical metric to evaluate the ability of myofibers to recover from injury [52]. Myofibers were visualized by staining tissue sections for LAMININ, an ECM component, while regenerated fibers were selected based on the presence of centrally located nuclei, a hallmark of injury-induced myogenesis. After segmenting and measuring myofibers using our recently developed myofiber segmentation pipeline [52], myofibers were false color-coded based on fiber size (Fig. 3b). Similar to IMAT, we found no difference in CSA in uninjured TAs between *Dhh*$^{-/-}$ and control mice arguing that DHH is also dispensable for embryonic myogenesis and adult maintenance (Fig. 3b and c). In contrast, myofiber CSA was significantly decreased 21 days post CTX injury in mice that have lost *Dhh* compared to controls (Fig. 3b and c). This reduction in average CSA is due to a change in distribution of fiber size, where *Dhh*$^{-/-}$ mice display a shift from larger to smaller fibers (Fig. 3d). Thus, loss of Dhh impairs myofiber regeneration. As an independent confirmation, we also treated wild type mice with Gant61 (Fig. 3e) and found a decrease in CSA 7 days post CTX injury (Fig. 3f and g) similar to loss of *Dhh*. Thus, the Hh pathway, induced by DHH, is critical for myofiber regeneration after an acute injury. Next, we sought to determine whether DHH was also required for muscle regeneration after a GLY-induced injury. We analyzed CSA 21 days after a GLY injury (Fig. 3h) and found no difference in myofiber size between *Dhh*$^{-/-}$ and controls (Fig. 3i and j). Together, our data indicates that an acute non-adipogenic injury requires DHH for efficient myofiber regeneration, but that DHH is dispensable for the recovery after a more chronic, adipogenic injury (Fig. 3k).

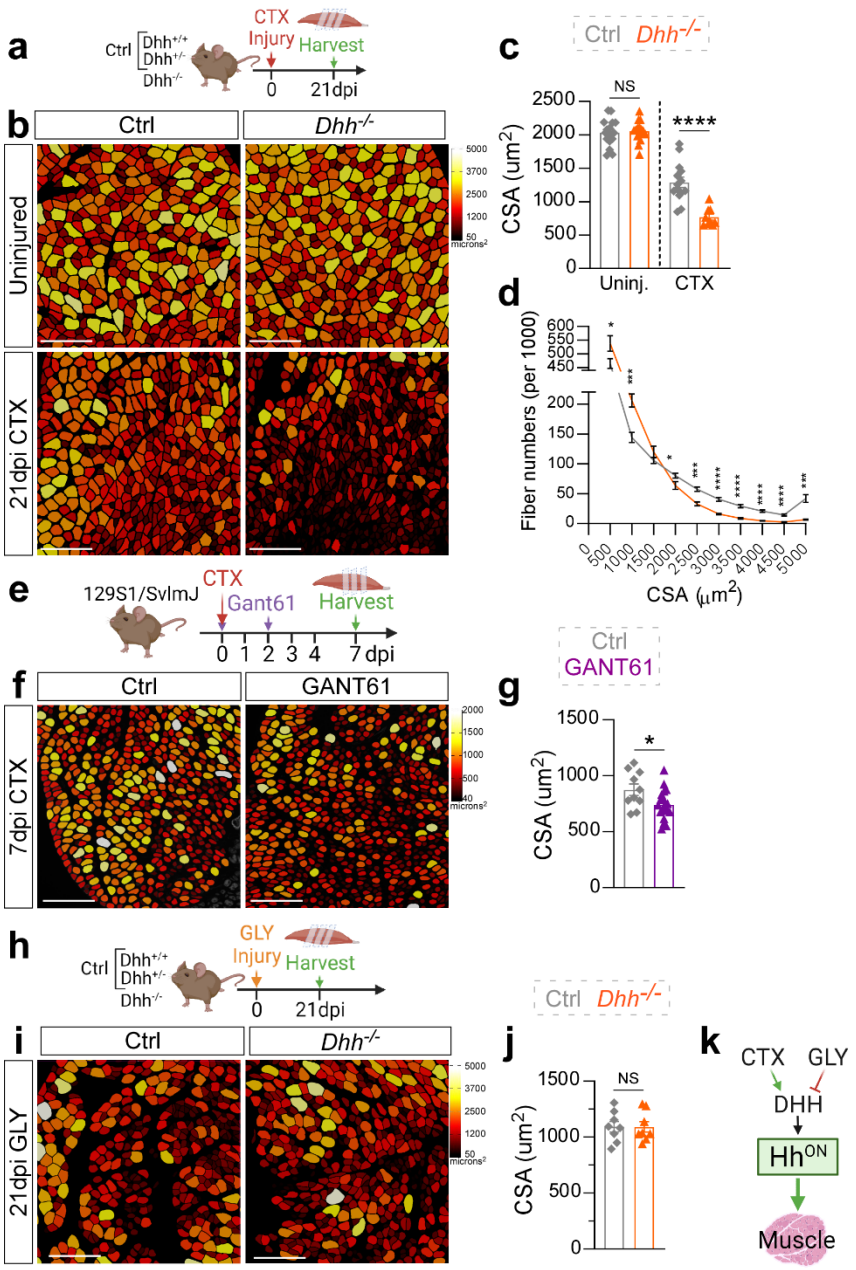

Figure 3. DHH is necessary for myofiber regeneration post injury. **a)** Experimental outline. **b)** Myofibers of *Dhh*$^{-/-}$ and ctrl mice color-coded based on cross sectional area (CSA). Scale bar: 250 μm. **c)** Average CSA (μm^2) of uninjured (n=16 TAs) and injured (n=9 TAs) *Dhh*$^{-/-}$ compared to uninjured (n=17 TAs) and injured (n=14 TAs) ctrl mice. **d)** Fiber number distribution based on their CSA (μm^2) in *Dhh*$^{-/-}$ and ctrl mice (same # as in c)). **e)** Experimental outline. **f)** Myofibers of Gant61- and vehicle treated mice 7 days post CTX injury. Myofibers were color-coded based on size, as in b). Scale bar: 250 μm. **g)** Average CSA (μm^2) of vehicle (n=10 TAs) and Gant61 (n=19 TAs) treated mice 7 days post CTX. **h)** Experimental outline. **i)** Myofibers of *Dhh*$^{-/-}$ and ctrl mice 21 days post GLY. Myofibers were color-coded as above. **j)** Average CSA (μm^2) of *Dhh*$^{-/-}$ (n=8 TAs) and ctrl (n=8 TAs) mice 21 days after GLY injury. **k)** *Model*: CTX, but not GLY, activates the Hh pathway through induction of DHH. Once active, Hh aids in myofiber regeneration. All data are represented as mean ± SEM. For c and g, an unpaired two-tailed t-test was used. For d, multiple unpaired two-tailed t-tests with a false discovery rate of 1 were used. A p value less than 0.05 was considered statistically significant where: * p≤ 0.05, ** p≤ 0.01, *** p≤ 0.001 and **** p≤ 0.0001.

<u>DHH controls IMAT formation through its downstream target Timp3</u>

IMAT forms through the differentiation of FAPs into fat cells, a process that requires ECM remodeling due to the activity of different MMPs (matrix metalloproteinases) [63, 64]. Our previous data highlighted that ectopic Hh activation inhibits IMAT formation through induction of *Timp3* (Tissue inhibitor of metalloproteinase 3), a secreted inhibitor of MMPs [8]. To test if loss of *Dhh* results in repression of *Timp3*, we evaluated the expression of *Timp3* in the *Dhh*$^{-/-}$ and control mice by RT-qPCR. As expected, we saw a significant reduction in *Timp3* expression 3- and 7-days post CTX injury (Fig. 4a). To functionally test whether DHH blocks IMAT through TIMP3, we determined whether the increase in IMAT in *Dhh*$^{-/-}$ mice could be rescued by treatment of Batimastat [8], a pharmacological mimetic of TIMP3 activity (Fig. 4b). By quantifying the number of PERILIPIN$^+$ adipocytes 7dpi after CTX injury, we found a significant increase in IMAT formation between control and *Dhh*$^{-/-}$ mice in the vehicle treated group (Fig. 4c and d) similar to Figure 2. Excitingly, treating *Dhh*$^{-/-}$ mice with Batimastat sufficiently blocked this ectopic IMAT formation (Fig. 4c and d). Thus, DHH controls IMAT formation via the induction of *Timp3*. Next, we asked if

Batimastat treatment would also rescue the myofiber regeneration defects observed after loss of *Dhh*. Comparing the cross-sectional area of myofibers between vehicle- and Batimastat-treated control and *Dhh*$^{-/-}$ mice, revealed that Batimastat treatment was not sufficient to rescue the impairment in myofiber regeneration upon loss of *Dhh* (Fig. 4c and e). Thus, DHH prevents IMAT formation through induction of *Timp3,* but controls myofiber regeneration through a TIMP3-independent mechanism (Fig. 4f).

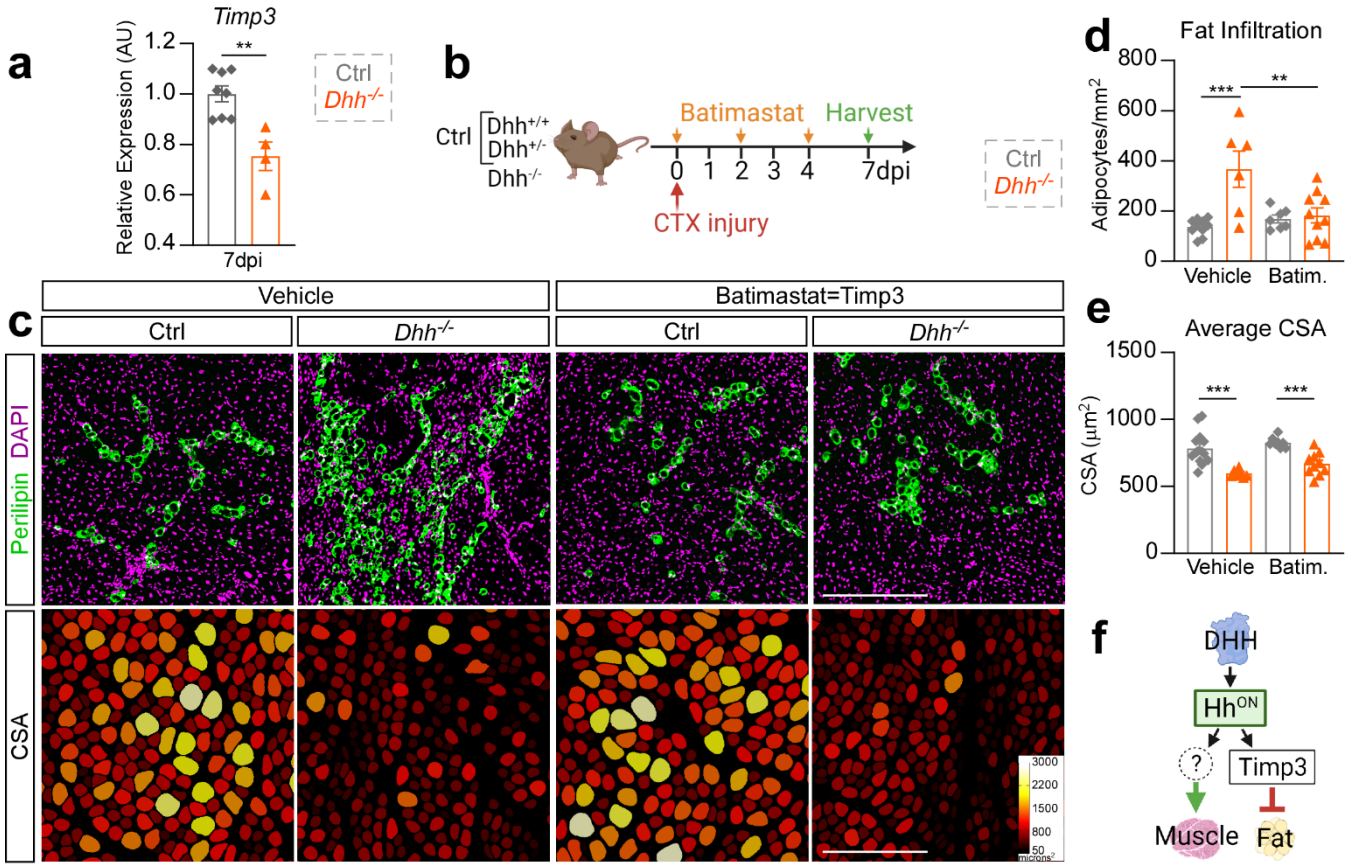

Figure 4. DHH controls IMAT formation but not muscle regeneration through TIMP3. a) RT-qPCR of whole muscle lysate for *Timp3* in *Dhh*$^{-/-}$ (n=4 TAs) and ctrl (n=8 TAs) mice 7 days post CTX injury. **b)** Experimental outline. **c)** Immunofluorescence for PERILIPIN^{+} adipocytes (green; top) and PHALLOIDIN^{+} myofibers (color coded based on CSA; bottom) 7 days post CTX injury of vehicle or batimastat treated *Dhh*$^{-/-}$ and ctrl mice. Scale bars: 250 µm. **d)** Adipocyte quantification of c (vehicle-treated *Dhh*$^{-/-}$ (n=6 TAs) and ctrl (n=10 TAs) in comparison to batimastat-treated *Dhh*$^{-/-}$ (n=10 TAs) and ctrl (n=7 TAs) mice). **e)** CSA measurements of c (vehicle-treated *Dhh*$^{-/-}$ (n=7 TAs) and ctrl (n=14 TAs) in comparison to batimastat-treated *Dhh*$^{-/-}$ (n=10 TAs) and ctrl (n=8 TAs) mice). **f)** *Model*: DHH represses IMAT, but not myogenesis, through induction of *Timp3*. All data are represented as mean ± SEM. For a), a paired two-tailed t-test was used. (d and e) A two-way ANOVA followed by Tukey's multiple comparison test was used. A p value less than 0.05 was considered statistically significant where: * p≤ 0.05, ** p≤ 0.01 and *** p≤ 0.001.

<u>Ectopic Hedgehog activation impairs both adipogenesis and myogenesis</u>

Our previous data demonstrated that Hh is sufficient to prevent IMAT formation and boost muscle regeneration [8], while our current results reveal that Hh is also necessary for both processes (Fig. 2). To determine the timing for when Hh activation is required during the regenerative process, we pharmacologically activated Hh signaling at different time points post CTX or GLY injury via administration of the Smoothened Agonist, SAG (Fig. S2a). To achieve sustained Hh activity, we administered SAG at days 0-, 2- and 4 post injury; while temporal activation was carried out by a single SAG dose either on the day of injury (0 dpi), 2 dpi, or 4 dpi (Fig. 5a). We confirmed Hh activation by measuring *Gli1* expression 7 days after injury via RT-qPCR. As expected, we observed highest Hh activation in both injury models when SAG was administered repetitively every other day (Fig. 5b). While *Gli1* levels returned to baseline at day 7 after a single dose of SAG at day of injury (0 dpi), Hh activation

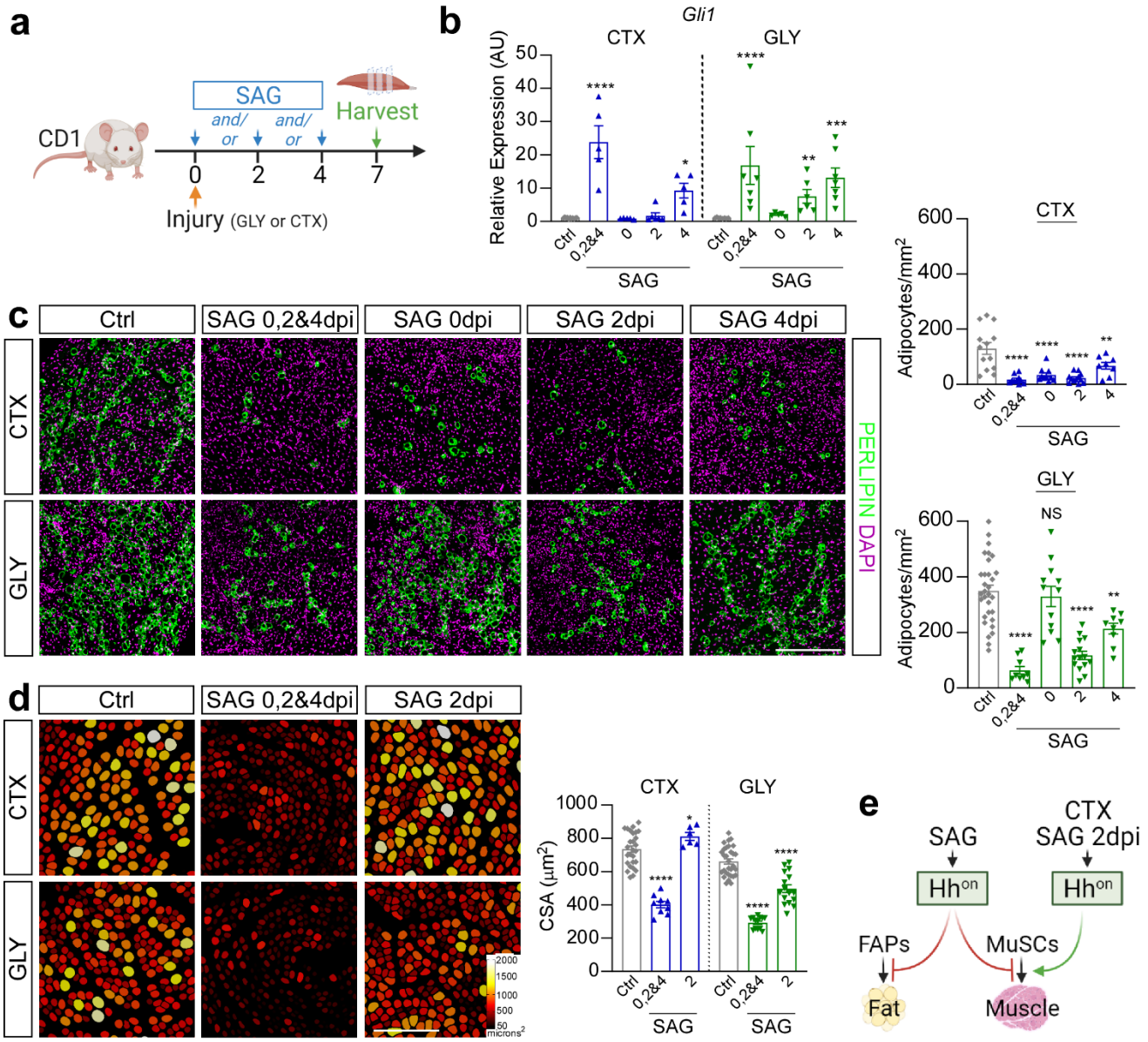

Figure 5. Hh controls IMAT formation and myofiber regeneration in an injury- and time-dependent manner. **a)** Experimental outline. **b)** RT-qPCR for *Gli1* 7 days post injury when treated with vehicle (CTX: n=11 TAs; GLY: n=8 TAs), SAG at 0-, 2- and 4 dpi (CTX: n=5 TAs; GLY: n=7 TAs), SAG at 0 dpi (CTX & GLY: n=5 TAs), SAG at 2 dpi (CTX & GLY: n=6 TAs) or SAG at 4 dpi (CTX: n=5 TAs; GLY: n=7 TAs). **c)** *(Left)* Immunofluorescence for PERILIPIN⁺ adipocytes (green) 7 days post CTX *(top)* or GLY *(bottom)* injury when treated with vehicle, SAG at 0-, 2- and 4 dpi, SAG at 0 dpi, SAG at 2dpi or SAG at 4 dpi. Nuclei were visualized with DAPI (purple). Scale bars 250 µm. Quantification of adipocytes from CTX (*right top*) and GLY (*right bottom*) 7 days post injury. Vehicle control (CTX: n=13 TAs; GLY: n=31 TAs), SAG at 0-, 2- and 4 dpi (CTX: n=10 TAs; GLY: n=9 TAs), SAG at 0 dpi (CTX & GLY: n=12 TAs), SAG at 2 dpi (CTX: n=12 TAs; GLY: n=15 TAs) or SAG at 4 dpi (CTX: n=8 TAs; GLY: n=9 TAs). **d)** *(Left)* Color-coded myofibers based on cross sectional area (CSA) of CTX *(top)* and GLY *(bottom)* injured mice treated with SAG at 0-, 2- and 4 dpi, and SAG at 2 dpi. Scale bars: 250 µm. *(Right)* Average CSA (µm²) 7 days post CTX injury. Vehicle control (CTX: n=27 TAs; GLY: n=30 TAs), SAG at 0-, 2- and 4 dpi (CTX: n=9 TAs; GLY: n=13 TAs), SAG at 2 dpi (CTX: n=6 TAs; GLY: n=17 TAs). **e)** *Model:* SAG -induced Hh activation blocks IMAT formation in both injures. Sustained Hh activation also impairs muscle regeneration, while a single bolus of SAG at day 2 post CTX, but not GLY, improves regeneration. All data are represented as mean ± SEM. (b-d) One- way ANOVA followed by a Dunnet's multiple comparison was used. A p value less than 0.05 was considered statistically significant where: * p≤ 0.05, ** p≤ 0.01, *** p≤ 0.001 and **** p≤ 0.0001.

was still significantly elevated when SAG was administered at day 4. Interestingly, we still detected high *Gli1* expression levels 5 days after SAG injection at 2 dpi post GLY injury while Hh activity was no longer elevated post CTX injury (Fig. 5b). These data suggest that the pharmacokinetics of Hh activity differs between the two injury types.

We next evaluated the effect of sustained versus temporal Hh activation on IMAT formation through quantification of PERILIPIN^{+} adipocytes. Confirming our and others previous work [51, 52, 53], GLY, compared to CTX, induced ~4-fold more IMAT (Fig. 5c). In the context of a CTX injury, sustained and temporal Hh activation significantly blocked IMAT formation, albeit to a lesser extent when activated at 4 dpi (Fig. 5c). In contrast, Hh activation displayed a narrower therapeutic time window in the GLY model. For example, IMAT post GLY was inhibited the strongest with sustained Hh activation, followed by SAG administration at 2 dpi, with only a modest anti-adipogenic impact when injected at day 4 (Fig. 5c). In contrast to CTX, there was no effect on IMAT formation when SAG was administered at the time of GLY injury (Fig. 5c). These data indicate that the time window where FAPs are susceptible to Hh-induced adipogenic repression is broadest for a CTX injury with a very narrow therapeutic window between 2- and 4-days post injury for GLY.

To determine if Hh activity is also required for myofiber regeneration, we assessed the size of PHALLOIDIN^{+} myofibers for various SAG dosing time points 7 days post CTX and GLY injury (Fig. 5d). In both injury models, sustained Hh activation and activation at day 4 post injury led to a decrease in average myofiber size, while no effect was observed when SAG was administered on the day of injury (Fig. 5d). Unexpectedly, Hh activation at 2 days post injury had opposing effects depending on the type of injury. Similar to two recent reports [40, 43], SAG administration post CTX promoted regenerative myogenesis (Fig. 5d) indicating that boosting Hh levels during acute injuries is beneficial. However, SAG administration at 2 days post GLY injury severely impaired myofiber regeneration. Thus, ectopic Hh activation can act as regenerative or degenerative signal depending on injury model and time window (Fig. 5e).

Our data indicate that a single SAG injection at 2 dpi causes prolonged Hh activation post GLY injury compared to CTX (Fig. 5b). To determine if the muscle regeneration defects we observed in the GLY model are due to sustained, high-level Hh activity, we administrated SAG at 0-, 2- and 4 days post GLY injury at different doses: 1x, 0.5x, 0.33x and 0.2x dose (Fig. S2b). Using RT-qPCR, we found a dose-dependent induction of *Gli1* expression (Fig. S2c). Quantifying the number of PERILPIN^{+} adipocytes, we detected a strong correlation between Hh levels and IMAT formation (Fig. S2d and e). Similarly, myofiber size, based on CSA measurements, was also inhibited in a dose-dependent manner (Fig. S2d and f). Thus, ectopic Hh activation post GLY injury blocks IMAT but also inhibits myofiber regeneration in a dose-dependent fashion.

<u>Hh activation within FAPs blocks IMAT and indirectly impairs regenerative myogenesis.</u>

How does ectopic Hh activation impact regeneration-induced myogenesis? As FAPs and MuSCs possess a primary cilium [43, 48, 49, 65, 66, 67], both cell types are capable of responding to either DHH or SAG. Therefore, Hh activation could impair myogenesis via a direct influence on MuSCs or indirectly through FAPs. To distinguish between the two possibilities, we used a conditional mouse model, which, upon Tamoxifen (TMX) administration, results in the genetic deletion of Ptch1, a negative regulator of the pathway, within FAPs (*Pdgfrα-Cre*ERT *Ptch1*$^{c/c}$, called FAP$^{no\ PTCH1}$). As we previously reported [8], loss of *Ptch1* results in FAP-specific ectopic Hh activation (Fig. 6a). Tamoxifen was administered to 12-week-old mice at two consecutive days by oral gavage, followed by a 2-week wash-out period before injuring TAs with GLY (Fig. 6a). We first evaluated IMAT formation by quantifying the number of PERILIPIN-expressing adipocytes. While there was no difference in the amount of IMAT in the absence of injury, IMAT formation is robustly blocked 21 days post GLY injury in FAP$^{no\ PTCH1}$ mice compared to littermate controls (Fig. 6b and S3b). These results confirm and extend our previous findings that IMAT formation remains repressed beyond 7 days post GLY injury upon FAP-specific Hh activation [8].

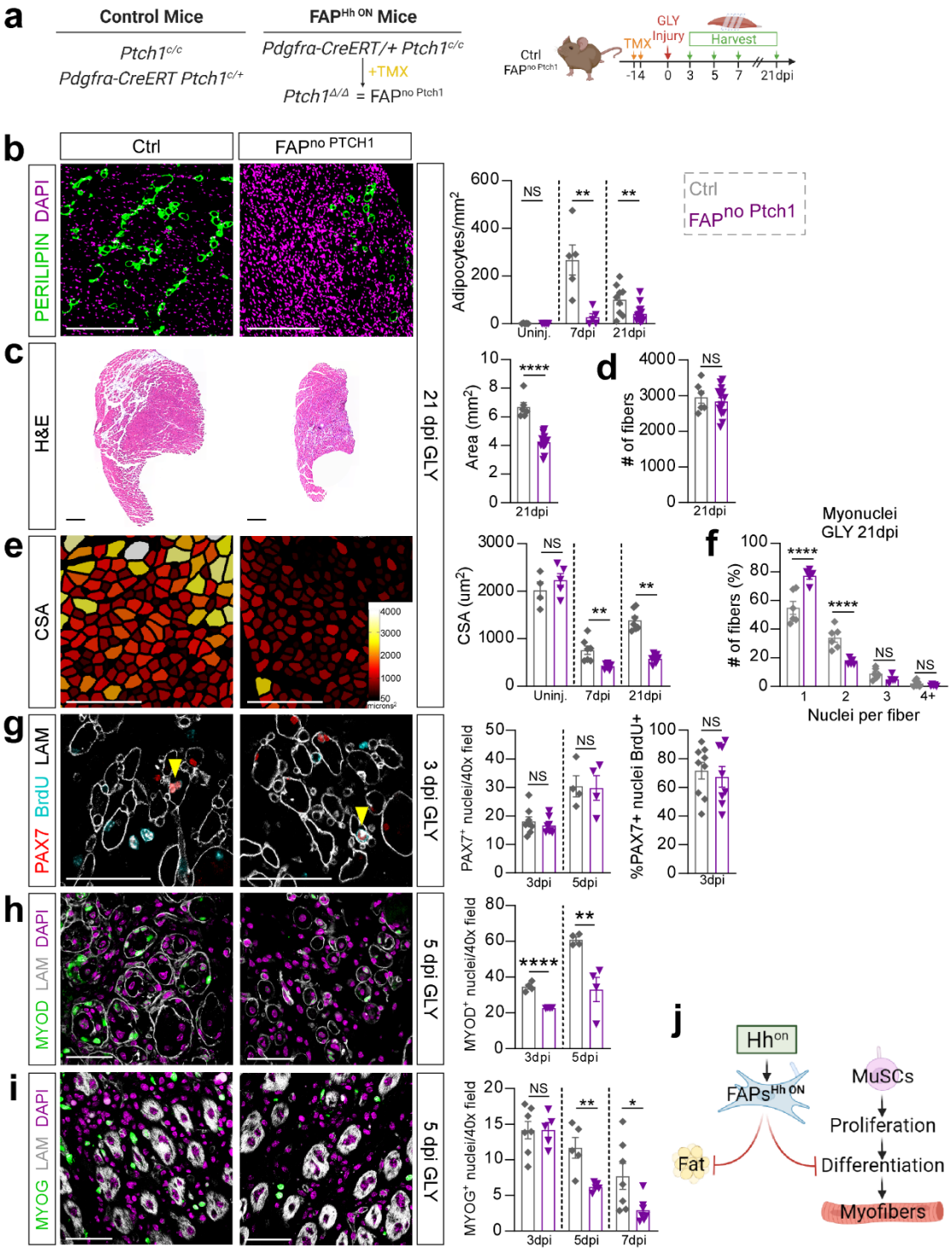

Figure 6. FAP-specific Hh activation severely impairs myofiber regeneration.
a) Experimental outline. **b)** *(Left)* Immunofluorescence for PERILIPIN+ adipocytes (green) 21 days post GLY. Nuclei stained for DAPI (purple). Scale bars: 250 µm. *(Right)* Quantification of adipocytes in uninjured FAP$^{no\ Ptch1}$ (n=5 TAs) and ctrl (n=5 TAs) mice, 7 days post GLY in FAP$^{no\ Ptch1}$ (n=5 TAs) and ctrls (n=5 TAs), and 21 days post GLY in FAP$^{no\ Ptch1}$ (n=14 TAs) and ctrls (n=9 TAs). **c)** *(Left)* Hematoxylin and Eosin (H&E) staining of FAP$^{no\ Ptch1}$ and ctrl mice 21 days post GLY. Scale bars: 500 µm. *(Right)* Quantification of total TA area (mm^2) 21 days post GLY of FAP$^{no\ Ptch1}$ (n=14 TAs) and ctrl (n=6 TAs) mice. **d)** Quantification of total fiber numbers 21 days post GLY of FAP$^{no\ Ptch1}$ (n=14 TAs) and ctrl (n=6 TAs) mice. **e)** *(Left)* Color-coded myofibers of FAP$^{no\ Ptch1}$ and ctrl mice. Scale bars: 250 µm. *(Right)* Average CSA (µm^2) of uninjured FAP$^{no\ Ptch1}$ (n=5 TAs) and ctrl (n=4 TAs) mice, 7 days post GLY of

FAP$^{no\ Ptch1}$ (n=7 TAs) and ctrl (n=7 TAs) mice and 21 days post GLY of FAP$^{no\ Ptch1}$ (n=9 TAs) and ctrl (n=7 TAs) mice. **f)** Percent distribution of myonuclei from FAP$^{no\ Ptch1}$ (n=5 TAs) and ctrl (n=6 TAs) mice. **g)** *(Left)* Immunofluorescence for PAX7 (MuSCs, red), BrdU (proliferating cells, cyan) and LAMININ (myofiber outline, white) 3 days post GLY. Arrowhead marks PAX7 BrdU double positive cells. Scale bars: 50 µm. *(Middle)* Quantification of total MuSCs (PAX7$^+$ nuclei) per 40x field of FAP$^{no\ Ptch1}$ mice 3- (n=8 TAs) and 5- (n=5 TAs) days post GLY, and ctrl mice 3 (n=8 TAs) and 5 dpi (n=5 TAs). *(Right)* Percent of proliferating MuSCs (% PAX7$^+$ nuclei over total BrdU$^+$ cells) 3 days post GLY in FAP$^{no\ Ptch1}$ (n=8 TAs) and ctrl (n=9 TAs) mice. **h)** *(Left)* Immunofluorescence of MYOD$^+$ (green) nuclei and LAMININ (white) 5 days post GLY. Nuclei marked by DAPI (purple). Scale bars: 50 µm. *(Right)* Quantification of MYOD$^+$ nuclei per 40x field of FAP$^{no\ Ptch1}$ mice 3- (n=4 TAs) and 5- (n=4 TAs) days post GLY injury, and ctrl mice 3 (n=4 TAs) and 5 dpi (n=4 TAs). **i)** *(Left)* Immunofluorescence of MYOG$^+$ nuclei (green) and myofibers (Phalloidin, white) of FAP$^{no\ Ptch1}$ and control mice 5 days post GLY injury. Scale bars: 50 µm. *(Right)* Quantifications of percent of MYOG$^+$ nuclei of FAP$^{no\ Ptch1}$ (3dpi, n=5 TAs; 5 dpi, n=5 TAs; 7 dpi, n=7 TAs) and ctrl mice (3dpi, n=7 TAs; 5 dpi, n=5 TAs; 7 dpi, n=7 TAs). **j)** *Model:* FAP-specific Hh activation prevents the adipogenic differentiation of FAPs. In addition, it impairs myofiber regeneration by preventing MuSC differentiation. All data are represented as mean ± SEM. (c-i) An unpaired two-tailed t test was used. A p value less than 0.05 was considered statistically significant where: * $p \leq 0.05$, ** $p \leq 0.01$, *** $p \leq 0.001$ and **** $p \leq 0.0001$.

However, by extending our analysis to 21 days post GLY injury we also noticed that TA muscles from FAP$^{no\ PTCH1}$ mice were significantly smaller compared to controls (Fig. 6c). Upon closer examination, while uninjured H&E-stained TAs were of comparable size between genotypes (Fig. S3c), there was a significant decrease in total area 21 days post GLY in TAs from FAP$^{no\ PTCH1}$ mice (Fig. 6c). To determine if the change in TA size is due to lack of myofiber regeneration, we quantified the number of myofibers present in TA cross sections in FAP$^{no\ PTCH1}$ and control mice as a proxy for the total number of fibers present per TA (Fig. 6d). We failed to detect any differences in the number of muscle fibers indicating that myofiber regeneration is still functional in FAP$^{no\ PTCH1}$ mice. Next, we asked if the TA size differences are due to delayed or incomplete myofiber regeneration resulting in smaller myofibers by measuring individual myofiber CSAs between genotypes (Fig. 6e). There was no difference in CSA without injury (Fig. 6e and S3d), highlighting that FAP-specific Hh activation is not required for myofiber maintenance. In contrast, while control mice display significant myofiber recovery from 7 to 21 days post GLY injury, FAP$^{no\ PTCH1}$ mice failed to increase the size of their myofibers and displayed a dramatic myofiber size shift towards smaller fibers (Fig. 6e and S3e). We further quantified the myonuclear content of each regenerated myofiber and found that FAP$^{no\ PTCH1}$ mice had significantly less myonuclei per fiber than controls (Fig. 6f). This suggests that FAP-specific Hh activation impairs myofiber regeneration in a cell non-autonomous fashion.

Upon muscle injury, MuSCs become activated, expand and transition along a stepwise process, controlled by pro-myogenic transcription factors such as MyoD and MyoG, to generate myoblasts. These myoblasts, in turn, continue to proliferate before differentiating into myocytes, and then fuse to either repair damaged or replace lost myofibers [3, 68]. To determine how Hh activation exclusively within FAPs impacts myofiber regeneration, we assessed the early steps of regeneration-induced myogenesis. For this, we harvested TAs 3-, 5- and 7 dpi post GLY injury from FAP$^{no\ PTCH1}$ and control mice (Fig. 6a). We first asked whether MuSC expansion was affected by determining the number of MuSCs and their proliferation rate. We administered Bromodeoxyuridine (BrdU), a thymidine analog that is incorporated during cell division, 2 hrs prior to harvesting and quantified the number of total PAX7$^+$ MuSCs and the number of PAX7 and BrdU double-positive MuSCs at 3- and 5 days post GLY. We detected no differences in either total MuSCs numbers or their proliferation rates at either time point (Fig. 6g). We next sought to evaluate if FAP-specific Hh activation affected the differentiation of MuSCs into myoblasts by assessing the number of cells expressing the pro-myogenic transcription factors MyoD and MyoG [69]. We quantified MYOD$^+$ nuclei and found a significant decrease in MYOD-expressing myoblasts in FAP$^{no\ PTCH1}$ mice compared to controls at both 3 and 5 dpi (Fig. 6h). This decrease in differentiation of MuSC was further corroborated by a decline in the number of MYOG$^+$ myocytes at 5 and 7 dpi (Fig. 6i). Thus, Hh activation in FAPs inhibits differentiation of MuSCs into myoblasts resulting in fewer myoblasts and myocytes. Together, FAP-specific Hh activation, while strongly inhibiting adipogenesis, severely impairs regenerative myogenesis by reducing the myoblast pool resulting in smaller myofibers (Fig. 6j).

Constitutive Hh activation causes FAPs to adopt a fibrotic fate

FAPs adopt both an adipogenic and fibrogenic fate during fatty fibrosis. However, it remains unknown how FAPs ultimately decide their fate. To determine if Hh signaling might affect the fibrogenic fate of FAPs, we assessed fibrosis in $FAP^{no\ PTCH1}$ and control littermates post GLY injury (Fig. 7a). We visualized collagen deposition through histological Sirius red staining 21 dpi (Fig. 7b). Compared to control, $FAP^{no\ Ptch1}$ mice displayed a massive upregulation of collagen (Fig. 7b). Thus, sustained, FAP-specific Hh activation pushes FAPs to adopt a fibrogenic fate leading to fibrosis. We next sought to investigate and compare the fibrotic effects of constitutive versus temporal Hh activation using SAG in both CTX and GLY injury models. Wild-type mice were injured with CTX or GLY and given SAG at either 0-, 2- and 4 dpi or only at 2 dpi (Fig. 7c). We found that repetitive Hh activation throughout the early stages of regeneration increased collagen content, independent of injury type (Fig. 7d), similar to that observed in $FAP^{no\ PTCH1}$ mice. Interestingly, we observed no difference in collagen deposition when SAG was administered 2 days post CTX or GLY injury (Fig. 7d).

We have previously shown that loss of FAP cilia resulted in Hh de-repression and subsequent low-level Hh activation due to loss of GLI repressor [8]. This low-level Hh activation was sufficient to inhibit adipogenesis and promote myogenesis. To determine if Hh de-repression also affects fibrosis, we assessed collagen content in mice that lack FAP cilia. In this mouse model, the gene *Ift88*, an essential ciliary component, is conditionally deleted from FAPs using a FAP-specific tamoxifen-inducible CreERT line (*Pdgfrα-Cre*ERT *Ift88*$^{c/-}$, called $FAP^{no\ cilia}$) (Fig. 7e) [8]. $FAP^{no\ cilia}$ and control mice were orally gavaged two weeks prior to GLY injury, and tissues were harvested 21 dpi (Fig. 7e). We found no difference in collagen deposition (Fig. 7f), suggesting that low-level Hh activation due to Hh de-repression does not affect fibrosis. Taken together, constitutive Hh activation, but not Hh de-repression, either genetically or pharmacologically, promotes fibrosis independent of injury (Fig. 7e). However, short term Hh activation at day 2 post injury has no effect on fibrosis, while this dosing routine still prevents IMAT formation (Fig. 5d) and promotes myogenesis post CTX injury (Fig. 5d).

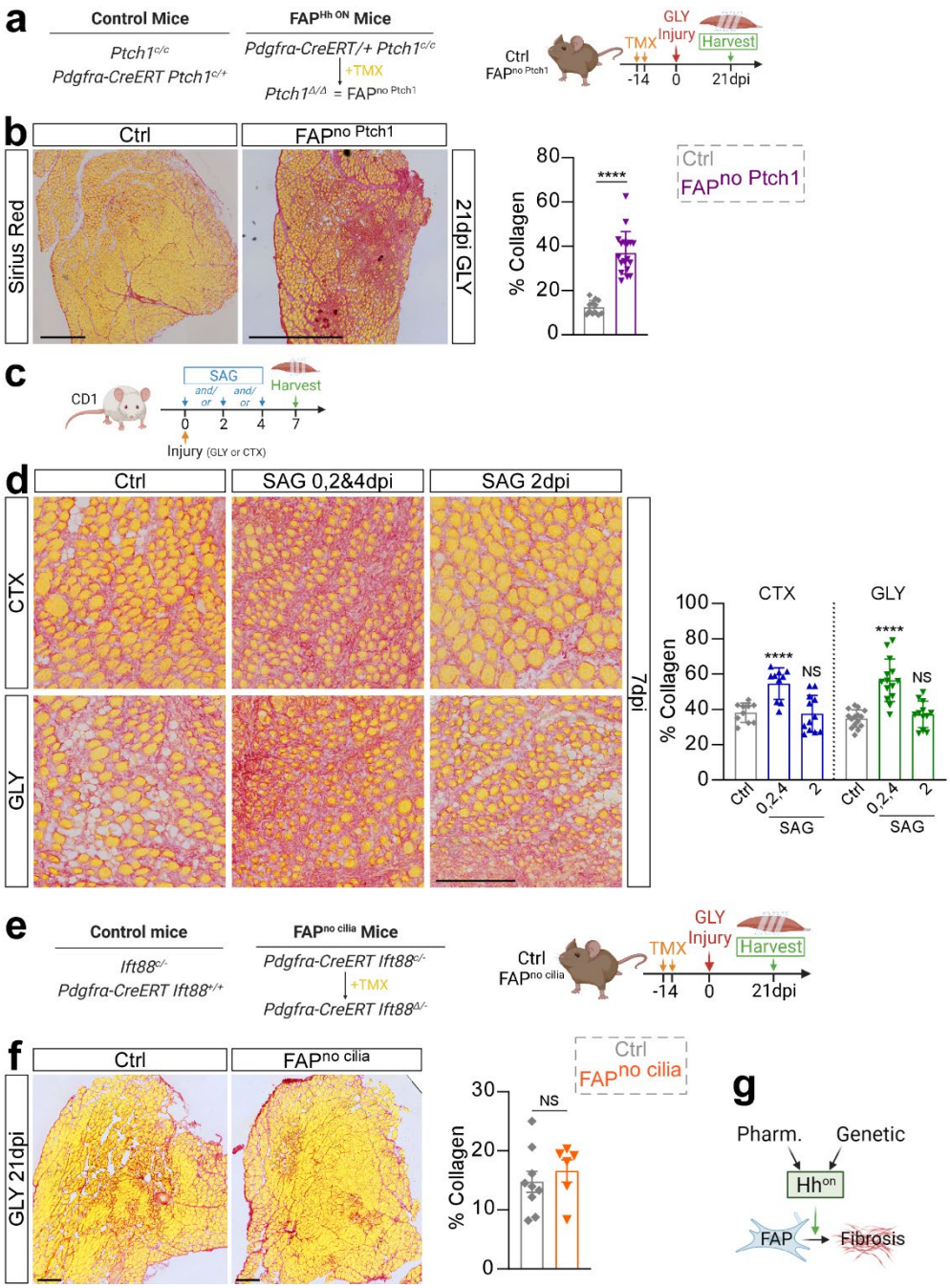

Figure 7. Sustained Hh activation promotes fibrosis. a) Experimental outline. **b)** Histological Sirius red staining *(left)* and quantification of percent of Sirius red-positive collagen (red, *right*) of FAP$^{no\ Ptch1}$ (n=18 TAs) and control (n=12 TAs) mice 21 dpi post GLY. Scale bars: 500 µm. **c)** Experimental outline. **d)** *(Left)* Sirius red staining 7 days after CTX *(top)* or GLY *(bottom)* injury after vehicle control, SAG at 0-, 2- and 4 dpi, and SAG at 2 dpi. Scale bars: 250 µm. *(Right)* Quantification of percent of Sirius red-positive collagen (red) 7 days after injury with vehicle control (CTX: n=10 TAs & GLY: n=15 TAs), SAG at 0-, 2- and 4 dpi (CTX: n=10 TAs & GLY: n=14 TAs) and SAG at 2 dpi (CTX & GLY: n=12 TAs). **e)** Experimental outline. **f)** Histological Sirius red staining *(left)* and quantification of percent of Sirius red-positive collagen (red, *right*) of FAP$^{no\ cilia}$ (n=6 TAs) and ctrl (n=8 TAs) mice, 21 days post GLY injury. Scale bars: 500 µm. **g)** *Model:* Sustained Hh activation through SAG, or genetically within FAPs, leads to increased fibrosis. However, fibrosis is not affected when Hh is punctually activated 2 dpi, independent of injury type, or through genetic de-repression in FAPs (not shown in model). All data are represented as mean ± SEM. (b; f) An unpaired two-tailed t test was used. d) One- way ANOVA followed by a Dunnet's multiple comparison was used. A p value less than 0.05 was considered statistically significant where: **** p≤ 0.0001.

Discussion

Increased IMAT infiltration with age and disease is strongly associated with decreased muscle strength and function [18, 20, 21, 22, 23, 24, 25, 26, 27, 28, 29]. However, it is still unclear whether IMAT forms due to the progressive loss of an adipogenic brake or the gradual gain of a pro-adipogenic trigger. We and others have previously demonstrated that ectopic Hh activation is a potent anti-adipogenic signal [8, 40]. Here, we identify Hh as an endogenous pathway that, through its ligand DHH, restricts IMAT formation and promotes muscle regeneration post injury (Fig 8). This significant discovery indicates that the pathological increase in IMAT may be due to loss of this adipogenic brake. At the same time, we show that the activity levels of Hh have a dramatic impact on the fate of FAPs. For example, while loss of Hh signaling promotes the adipogenic conversion of FAPs, high level activation blocks adipogenesis and pushes FAPs to adopt a myofibroblast fate resulting in fibrosis. Similarly, we also demonstrate that Hh signaling both promotes and restricts muscle regeneration depending on the level and timing of activation, and the type of injury. Together, we describe novel cell autonomous and non-autonomous roles for Hh signaling in controlling adipogenesis, fibrogenesis and post-regenerative myogenesis. This has major implications for the development of novel therapeutics for tissues affected by fatty fibrosis.

The Hh ligands, SHH and DHH, have both been proposed to be involved in skeletal muscle [35, 36, 37, 38]. However, which Hh ligand is responsible for muscle regeneration remained unclear. By querying scRNAseq data sets, we objectively identified DHH as the main ligand being expressed by endothelial and Schwann cells confirming our and others previous work [8, 38, 46, 47]. Recently, DHH has been shown to be required for neo-angiogenesis post ischemic hindlimb injury [38, 47]. However, it was unknown if DHH is also necessary for IMAT formation and/or muscle regeneration after an acute muscle injury. Using a genetic DHH null mouse model and two independent Hh antagonists, we found that DHH is the main ligand that induces Hh signaling in skeletal muscle. Once active, Hh restricts IMAT formation through induction of the anti-adipogenic factor TIMP3. DHH-induced Hh signaling also promotes muscle regeneration, however independent of TIMP3. Supporting our data, Kang et al, recently described that the cytokine Interleukin 15 (IL15) acts upstream of DHH and induces its expression [70]. Fittingly, IL15 activation also represses IMAT and enhances myofiber regeneration phenocopying active Hh signaling. Together, our results demonstrate that DHH plays novel anti-adipogenic and pro-myogenic roles during postnatal tissue repair.

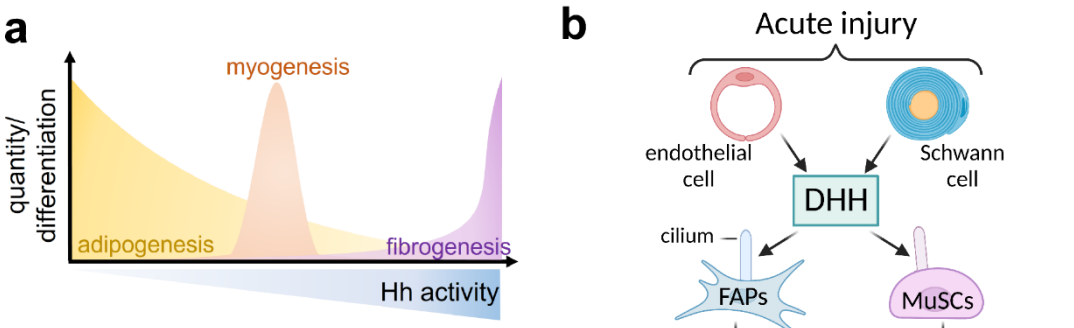

Figure 8. Hh signaling, via DHH, is crucial for balancing muscle regeneration and fatty fibrosis. a) *Hh activity levels control multiple cellular events.* Hh is a potent endogenous anti-adipogenic brake and its activity levels negatively correlate with IMAT formation. In addition, too little or too much Hh activity impairs muscle regeneration, while only a short pulse of Hh activity at the right time is beneficial. Last, sustained high-level Hh activation causes extensive fibrosis. regulates adult myogenesis directly via its influence on MuSCs.
b) *Hh signaling, via its ligand DHH, is required for successful muscle regeneration*: Following an acute but not adipogenic injury, endothelial and Schwann cells induce *Dhh*, which is then sensed by cilia on FAPs and MuSCs. Hh activation within FAPs leads to expression of *Timp3*, which blocks adipogenesis cell autonomously. Additionally, FAP-specific Hh activation controls myogenesis through a TIMP3-independent but cell non-autonomous mechanism. Hh also regulates adult myogenesis directly via its influence on MuSCs.

How does DHH control myofiber regeneration? The two main cell populations that carry a primary cilium, and thereby can respond to DHH, are FAPs and MuSCs [43, 48, 65, 66, 67]. Fittingly, we found that both cell populations display an active Hh signature indicating that they sense DHH. While our understanding of the role of cilia and ciliary Hh signaling in MuSCs is still evolving, recent findings demonstrate that MuSCs cilia control the balance between quiescence, self-renewal and proliferation [43, 44, 48, 65, 67]. Thus, Hh signaling may directly influence the myogenic compartment explaining why loss of *Dhh* results in impaired muscle regeneration. However, more experiments are needed to fully unravel the role of DHH and Hh signaling in MuSCs.

Although our data cannot exclude a direct myogenic influence of Hh, they provide compelling evidence that Hh can control muscle regeneration cell non-autonomously via its impact on FAPs. FAP-specific Hh activation severely impaired muscle regeneration by blocking myoblast differentiation, mimicking the phenotype of global Hh activation via the Hh agonist SAG. These data argue that ectopic Hh activation induces an anti-myogenic signal in FAPs. At the same time, the $FAP^{no\ PTCH1}$ data also conflict with our previous results where we found that FAP-specific, but low-level, Hh activation blocks IMAT formation and enhances muscle regeneration [8]. There, we demonstrated that cilia guard GLI3 repressor levels in FAPs. More specifically, removing FAP cilia resulted in loss of GLI3-R leading to Hh de-repression and low-level Hh activation [8]. Similar to our $FAP^{no\ PTCH1}$ data, this resulted in de-repression of TIMP3, which in turn inhibited the adipogenic differentiation of FAPs via changes to the ECM composition [8]. However, low-level Hh activation improved muscle regeneration [8]. This is in direct contrast to high-level Hh activation in our $FAP^{no\ PTCH1}$ mice, which, compared to our previous studies, resulted in severely compromised myogenesis. To determine if the levels of Hh activation matter, we attempted to mimic low versus high Hh activity levels by administering our Hh agonist at various concentrations. However, we failed to detect any beneficial myogenic effects at lower doses. Therefore, it is likely that Hh de-repression versus full Hh activation may induce different myogenic factors that either positively or negatively affect myogenesis. Fittingly, the number of genes being repressed in the Hh OFF state is much larger than the ones that are being induced in the Hh ON state [71]. Furthermore, it remains to be determined whether endogenous Hh activation in FAPs, via DHH, has any effect on muscle regeneration. Evidence for this being a possibility comes from a recent cell ablation approach [40]. Ablating Hh-responsive FAPs from muscle resulted in impaired muscle regeneration indicating that Hh does induce pro-myogenic factors in FAPs.

We also found that ectopic Hh activation, either global or specifically in FAPs, shifted FAPs away from an adipogenic to a fibrogenic fate resulting in massive scar tissue formation. In contrast, we did not observe any changes in fibrosis when we turned Hh OFF by removing *Dhh*. Thus, while Hh is sufficient to induce fibrosis, it is not necessary. As fibrotic scar tissue is a potent anti-myogenic signal [11, 72, 73], this increased fibrosis could also contribute to the myogenic defects we observe after ectopic Hh activation. We also determined whether Hh de-repression could result in fibrosis. However, we failed to detect any fibrotic changes after loss of FAP cilia. This is another example where Hh de-repression does not equal full Hh activation. Together, chronic high-level Hh activation induces muscle fibrosis. However, the role of Hh in tissue fibrosis needs further clarification as Hh signaling can act both as anti-fibrotic and pro-fibrotic signal depending on the tissue and type of injury [39, 74, 75, 76, 77].

When is DHH required during the regenerative process? By administrating the Hh agonist SAG at different time points post injury, we were able to determine the time windows for when Hh is required. We found that, although CTX has an earlier Hh-sensitive window, Hh activation at 2 days post GLY and CTX injury caused the largest repression of IMAT. Interestingly, our data also demonstrated that activation of Hh at day 2 affected fibrosis the most in both injuries suggesting that the influence of Hh on the fate of FAPs is strongest at day 2. This timing fits with our previous observations that early pro-adipogenic genes can be detected as early as 3 dpi with the first visible lipid droplets by day 5 [8]. This suggests that ectopically elevating Hh signaling pushes FAPs from an adipogenic to a fibrogenic fate resulting in reduced IMAT and increased fibrosis. In contrast, we find that Hh activation has both positive and negative effects on muscle regeneration depending on injury type and time. For example, SAG

administration impairs muscle regeneration at days 2 and 4 post GLY injury. In contrast, Hh activation at day 2 post CTX boosted myofiber regeneration, similar to findings from a recent report [40], while SAG at day 4 after CTX inhibited myogenesis similar to GLY. One possible explanation for this is that, because Hh signaling is already being induced after a CTX injury, the system is primed to respond to Hh compared to GLY, where Hh is being inactivated [8]. Boosting Hh activity via SAG may therefore enhance its beneficial effects. In addition, CTX and GLY cause different kinetic responses, which could explain the differences in timing requirement and phenotypic consequences. For example, CTX causes an earlier immune [78] and pro-fibrotic [51] response compared to GLY. Similarly, while CTX displays stronger myofiber degeneration at early injury stages, myofiber regeneration is less efficient with GLY [51, 52]. Together, our data indicate that Hh signaling has a very narrow potential therapeutic window that is dependent on injury type.

This work reveals that the Hh pathway, through its ligand DHH, is sufficient and necessary to restrict IMAT formation. The gradual loss of this endogenous adipogenic brake provides an attractive explanation for why pathological IMAT forms especially as Hh activity is severely blunted with age and disease [35, 36, 37, 39, 43]. We also uncovered that Hh acts both as a pro- and anti-myogenic signal and controls muscle regeneration through both cell autonomous and non-autonomous mechanisms. Thus, the Hh pathway remains an attractive therapeutic avenue, but further studies are needed to determine optimal dosing and timing, in addition to identifying the downstream targets through which Hh controls fibrosis and post-regenerative myogenesis.

Acknowledgements

We thank the members of the Kopinke laboratory for helping with data collections and critical reading of the manuscript. We also thank Karyn Esser and David Hammers for their valuable input on the manuscript. We greatly appreciate the sharing of CD1 mice by Margaret Hull and sharing of the *Pdgfra*^{CreERT} allele by Gabrielle Kardon. This study would have been impossible without Colin Dinsmore, who was the first to ask, “So, which Hh ligand is responsible?”. Last, we are immensely grateful for the unwavering support and mentoring of Jeremy Reiter. This work was supported by the US National Institutes of Health (NIH) grants NIH grant 1R01AR079449 to DK, R01AG058630 to BDC, T32HD043730 to AMN and T32EB023860 to DWM. The content is solely the responsibility of the authors and does not necessarily represent the official views of the NIH. Models were created with Biorender.

Author contributions

A.M.N. and D.K. designed the experiments and wrote the manuscript. A.M.N., C.D.J., L.Y.Z & A.A. performed the experiments and analyzed data. D.W.M. and B.D.C. designed and analyzed the RNAseq data. All authors discussed the results and commented on the manuscript.

Material & Correspondence

All correspondence and material requests should be addressed to dkopinke@ufl.edu.

Competing interests

The authors declare no competing interests.

Supplementary Figures:

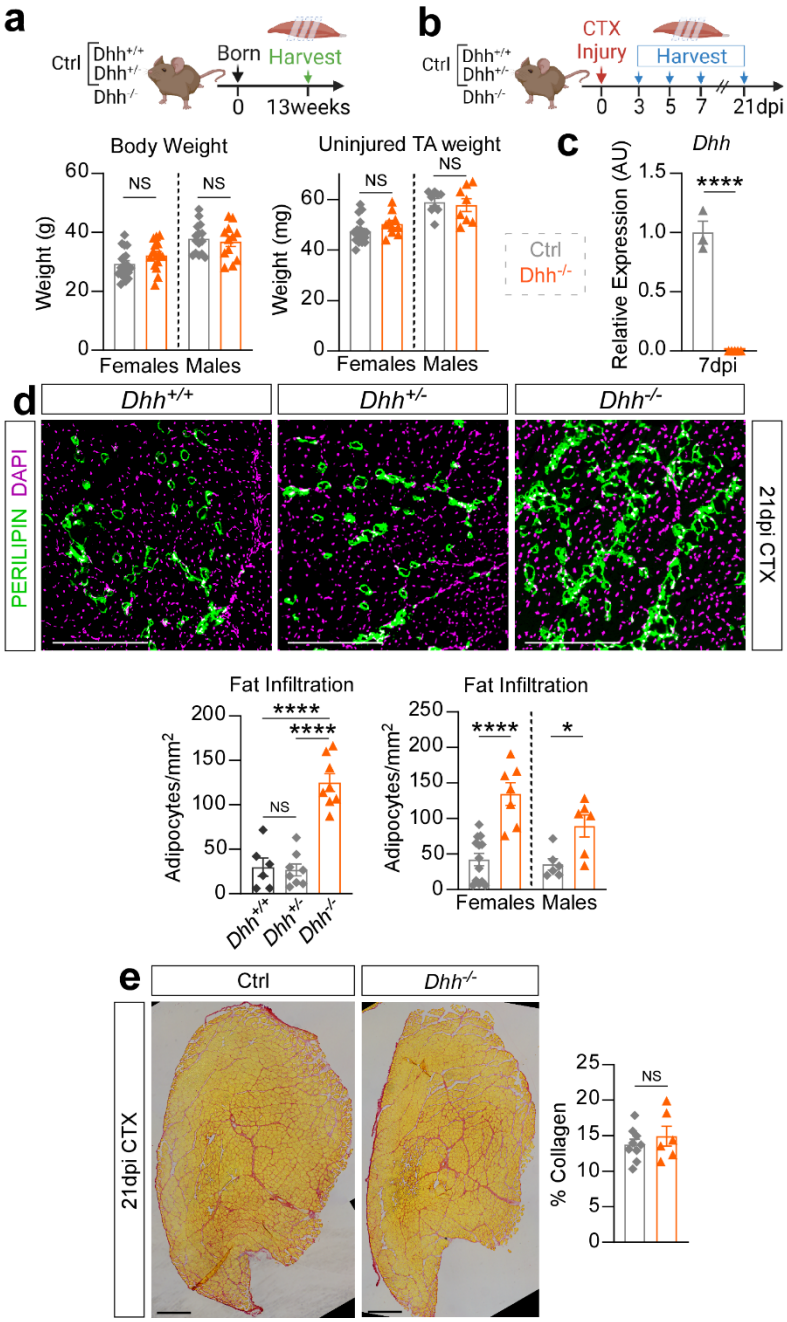

Figure S1. DHH regulates IMAT independent of fibrosis/Validation of the *Dhh*$^{-/-}$ mouse model. a) *(Top)* Experimental outline. *(Bottom Left)* Body weight (g) of 13-week-old *Dhh*$^{-/-}$ and ctrl mice (*Dhh*$^{-/-}$ females, n=15 mice; males, n=12 mice. Ctrl females, n=19 mice; males n=15 mice). *(Bottom Right)* Wet-weight of uninjured TAs (mg) of *Dhh*$^{-/-}$ and ctrl mice (*Dhh*$^{-/-}$ females, n=10 TAs; males, n=8 TAs. Ctrl females, n=17 TAs; males n=9 TAs). **b)** Experimental outline. **c)** RT-qPCR of *Dhh* expression 7 days after CTX injury of *Dhh*$^{-/-}$ (n=5 TAs) and ctrl (n=3 TAs) mice. **d)** *(Top)* Immunofluorescence of adipocytes (PERILIPIN^{+}, green) 21 days post CTX injury of *Dhh*$^{+/+}$, *Dhh*$^{+/-}$ and *Dhh*$^{-/-}$ mice. Nuclei were visualized with DAPI (purple). Scale bars: 250 µm. *(Bottom Left)* Quantification of adipocytes per uninjured are (mm^2) 21 days post CTX injury in *Dhh*$^{+/+}$, *Dhh*$^{+/-}$ and *Dhh*$^{-/-}$ mice. *(Bottom Right)* Adipocyte quantification of *Dhh*$^{-/-}$ and ctrl mice separated by sex. **e)** *(Left)* Histological Sirius red staining 21 days post CTX injury in *Dhh*$^{-/-}$ and ctrl mice. Scale bars: 500 µm. *(Right)* Quantification of percent of collagen (red) 21 dpi in *Dhh*$^{-/-}$ (n=6 TAs) and ctrl mice (n=9 TAs). All data are represented as mean ± SEM. (a, c-e) An unpaired two-tailed t test was used. A p value less than 0.05 was considered statistically significant where: * p≤ 0.05, ** p≤ 0.01, *** p≤ 0.001 and **** p≤ 0.0001.

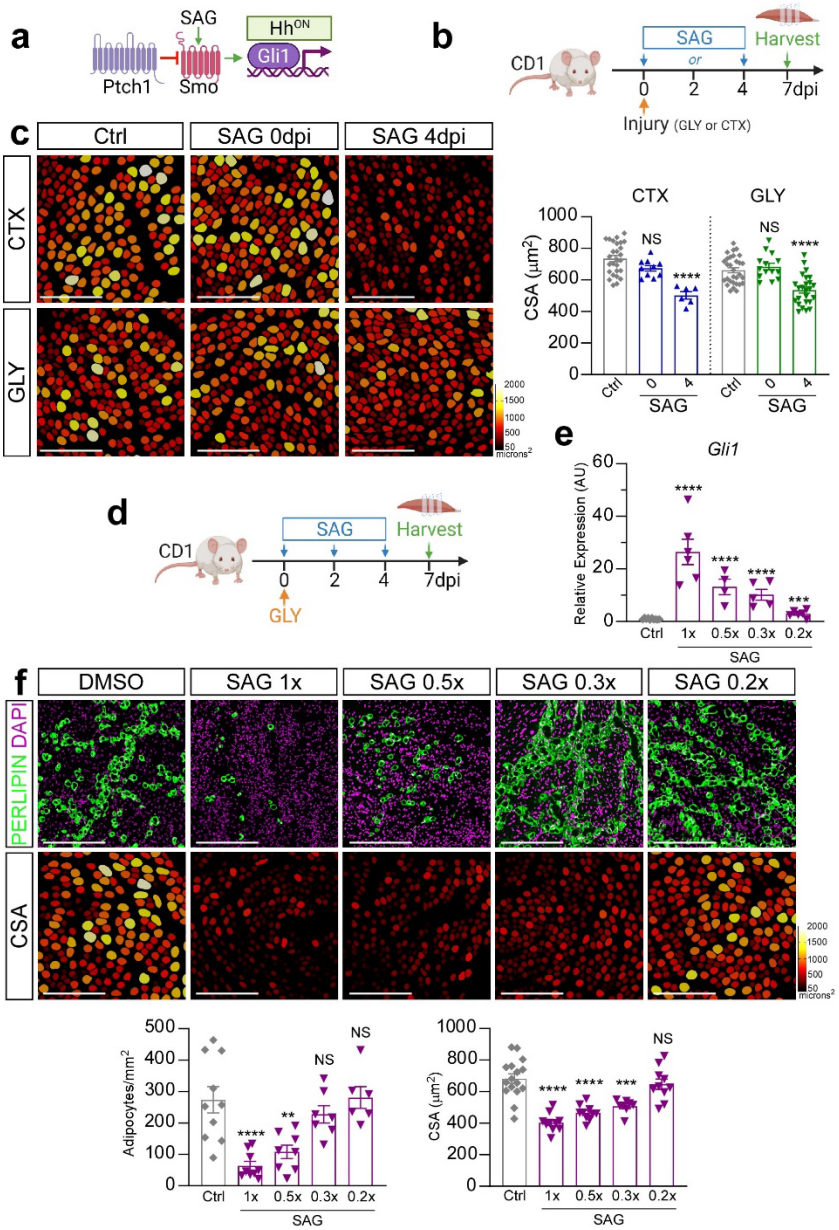

Figure S2. SAG influences adipogenesis and myogenesis in a dose- and time-dependent manner. a) SAG is a Smoothened (Smo) agonist overriding the repressive effect of Ptch1 resulting in Hh activation. **b)** Experimental outline. **c)** *(Left)* Color-coded myofibers based on cross sectional area (CSA) after CTX *(top)* or GLY *(bottom)* treated with vehicle control, SAG at 0 dpi and SAG at 4 dpi. Scale bars: 250 µm. *(Right)* Average CSA (µm^2) quantifications 7 days post injury with vehicle control (CTX & GLY: n=10 TAs), SAG at 0 dpi (CTX: n=10 TAs & GLY: n=14 TAs) and SAG at 4 dpi (CTX: n=6 TAs & GLY: n=25 TAs). To note, these time points are part of the experiment described in Figure 5 and, thus the same controls were used. **d)** Experimental outline. **e)** RT-qPCR of *Gli1* expression 7 days post GLY after treatment with vehicle control (n=10 TAs), SAG 1x (n=6 TAs, SAG 0.5x (n=4 TAs), SAG 0.3x (n=5 TAs) and SAG 0.2x (n=6 TAs). **f)** Vehicle control, SAG 1x, SAG 0.5x, SAG 0.3x and SAG 0.2x treated mice 7 days post GLY injury. *(Top)* Immunofluorescence of adipocytes (PERILIPIN$^+$, green). Nuclei visualized with DAPI (purple). *(Bottom)* Color-coded myofibers based on cross sectional area (CSA). Scale bars: 250 µm. **g)** *(Left)* Quantification of adipocytes per uninjured area (mm^2) 7 days post GLY injury of vehicle control (n=10 TAs), SAG 1x (n=9 TAs), SAG 0.5x (n=8 TAs), SAG 0.3x (n=7 TAs), and SAG 0.2x (n=6 TAs). *(Right)* Average CSA (µm^2) 7 days after GLY injury of vehicle control (n=16 TAs), SAG 1x (n=10 TAs), SAG 0.5x (n=11 TAs), SAG 0.3x (n=8 TAs), and SAG 0.2x (n=10 TAs). All data are represented as mean ± SEM. (c, e, g) One- way ANOVA followed by a Dunnet's multiple comparison was used. A p value less than 0.05 was considered statistically significant where: * p≤ 0.05, ** p≤ 0.01, *** p≤ 0.001 and **** p≤ 0.0001.

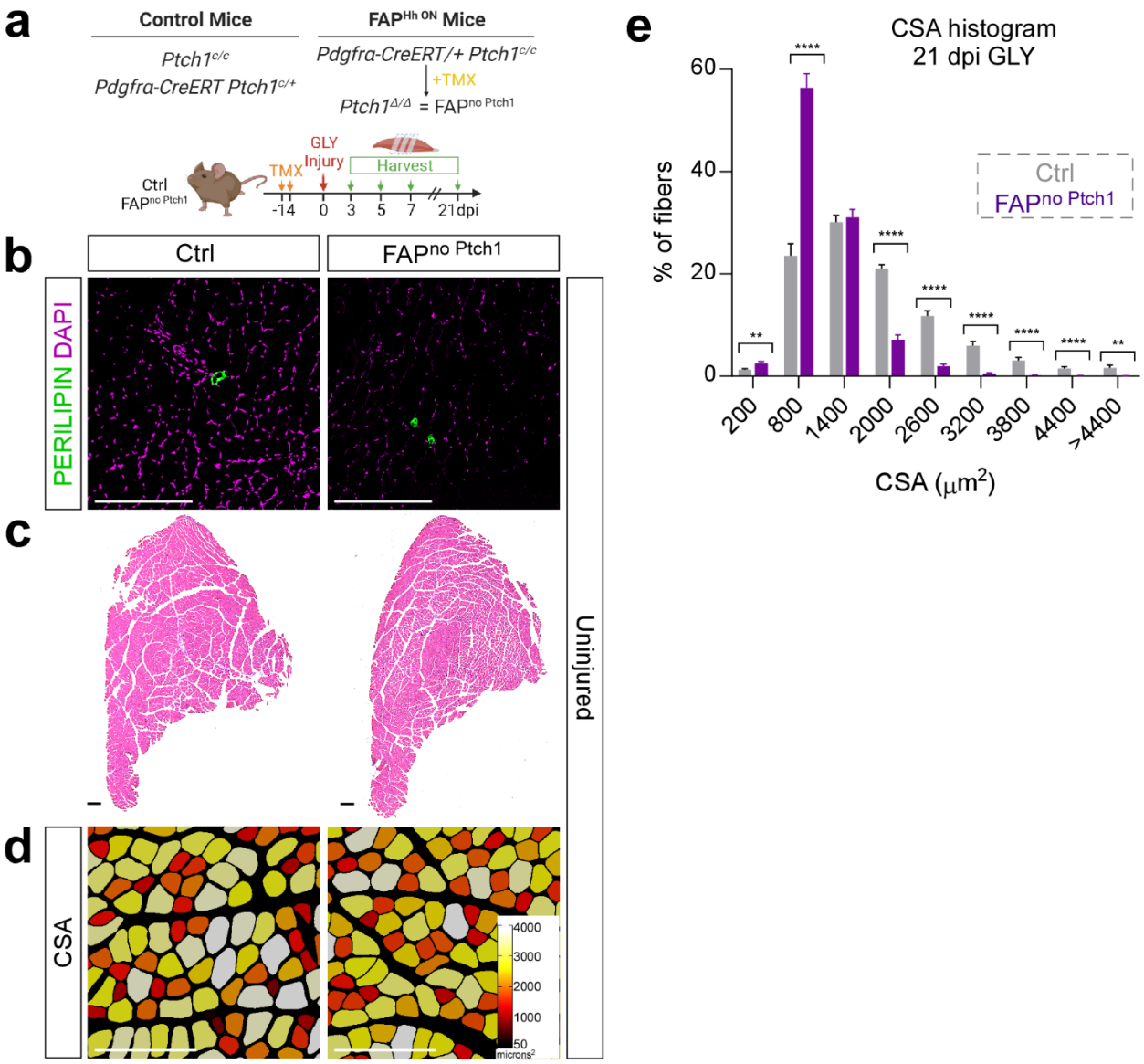

Figure S3. Genetic activation of Hh within FAPs impairs myogenesis. a) Experimental outline. **b)** Immunofluorescence of PERILIPIN^{+} adipocytes (green) of uninjured FAP$^{no\ Ptch1}$ and control mice. Scale bars: 250 µm. **c)** Hematoxylin and Eosin (H&E) staining of uninjured FAP$^{no\ Ptch1}$ and control mice. Scale bars: 500 µm. **d)** Color-coded myofibers based on cross sectional area (CSA) of uninjured FAP$^{no\ Ptch1}$ and control mice. Scale bar: 250 µm. **e)** Fiber number distribution based on their CSA (µm^2) in FAP$^{no\ Ptch1}$ (n= 19 TAs) and ctrl mice (n=14 TAs) 21 days post GLY injury. All data are represented as mean ± SEM. e) A two-way ANOVA followed by Tukey's multiple comparison test was used. A p value less than 0.05 was considered statistically significant where: * p≤ 0.05, ** p≤ 0.01, *** p≤ 0.001 and **** p≤ 0.0001.

References:

1. Lepper C, Partridge TA, Fan CM. An absolute requirement for Pax7-positive satellite cells in acute injury-induced skeletal muscle regeneration. *Development* **138**, 3639-3646 (2011).

2. Murphy M, Kardon G. Origin of vertebrate limb muscle: the role of progenitor and myoblast populations. *Curr Top Dev Biol* **96**, 1-32 (2011).

3. Relaix F, Zammit PS. Satellite cells are essential for skeletal muscle regeneration: the cell on the edge returns centre stage. *Development* **139**, 2845-2856 (2012).

4. Sambasivan R*, et al.* Pax7-expressing satellite cells are indispensable for adult skeletal muscle regeneration. *Development* **138**, 3647-3656 (2011).

5. Contreras O, Rossi FMV, Theret M. Origins, potency, and heterogeneity of skeletal muscle fibro-adipogenic progenitors-time for new definitions. *Skeletal Muscle* **11**, 16 (2021).

6. El Agha E*, et al.* Mesenchymal Stem Cells in Fibrotic Disease. *Cell Stem Cell* **21**, 166-177 (2017).

7. Joe AW*, et al.* Muscle injury activates resident fibro/adipogenic progenitors that facilitate myogenesis. *Nat Cell Biol* **12**, 153-163 (2010).

8. Kopinke D, Roberson EC, Reiter JF. Ciliary Hedgehog Signaling Restricts Injury-Induced Adipogenesis. *Cell* **170**, 340-351.e312 (2017).

9. Santini MP*, et al.* Tissue-Resident PDGFRalpha(+) Progenitor Cells Contribute to Fibrosis versus Healing in a Context- and Spatiotemporally Dependent Manner. *Cell Reports* **30**, 555-570 e557 (2020).

10. Uezumi A*, et al.* Mesenchymal Bmp3b expression maintains skeletal muscle integrity and decreases in age-related sarcopenia. *The Journal of Clinical Investigation* **131**, (2021).

11. Murphy MM, Lawson JA, Mathew SJ, Hutcheson DA, Kardon G. Satellite cells, connective tissue fibroblasts and their interactions are crucial for muscle regeneration. *Development* **138**, 3625-3637 (2011).

12. Wosczyna MN*, et al.* Mesenchymal Stromal Cells Are Required for Regeneration and Homeostatic Maintenance of Skeletal Muscle. *Cell Reports* **27**, 2029-2035 e2025 (2019).

13. Lukjanenko L*, et al.* Aging Disrupts Muscle Stem Cell Function by Impairing Matricellular WISP1 Secretion from Fibro-Adipogenic Progenitors. *Cell Stem Cell* **24**, 433-446 e437 (2019).

14. Uezumi A, Fukada S, Yamamoto N, Takeda S, Tsuchida K. Mesenchymal progenitors distinct from satellite cells contribute to ectopic fat cell formation in skeletal muscle. *Nat Cell Biol* **12**, 143-152 (2010).

15. Uezumi A*, et al.* Fibrosis and adipogenesis originate from a common mesenchymal progenitor in skeletal muscle. *J Cell Sci* **124**, 3654-3664 (2011).

16. Liu W, Liu Y, Lai X, Kuang S. Intramuscular adipose is derived from a non-Pax3 lineage and required for efficient regeneration of skeletal muscles. *Dev Biol* **361**, 27-38 (2012).

17. Scott RW, Arostegui M, Schweitzer R, Rossi FMV, Underhill TM. Hic1 Defines Quiescent Mesenchymal Progenitor Subpopulations with Distinct Functions and Fates in Skeletal Muscle Regeneration. *Cell Stem Cell* **25**, 797-813.e799 (2019).

18. Hogarth MW*, et al.* Fibroadipogenic progenitors are responsible for muscle loss in limb girdle muscular dystrophy 2B. *Nature Communications* **10**, 2430 (2019).

19. Stumm J*, et al.* Odd skipped-related 1 (Osr1) identifies muscle-interstitial fibro-adipogenic progenitors (FAPs) activated by acute injury. *Stem Cell Research* **32**, 8-16 (2018).

20. Milad N, White Z, Tehrani AY, Sellers S, Rossi FMV, Bernatchez P. Increased plasma lipid levels exacerbate muscle pathology in the mdx mouse model of Duchenne muscular dystrophy. *Skeletal Muscle* **7**, 19 (2017).

21. Goodpaster BH*, et al.* Obesity, regional body fat distribution, and the metabolic syndrome in older men and women. *Archives of Internal Medicine* **165**, 777-783 (2005).

22. Goodpaster BH*, et al.* Association between regional adipose tissue distribution and both type 2 diabetes and impaired glucose tolerance in elderly men and women. *Diabetes Care* **26**, 372-379 (2003).

23. Goodpaster BH*, et al.* The loss of skeletal muscle strength, mass, and quality in older adults: the health, aging and body composition study. *The Journals of Gerontology, Series A: Biological Sciences and Medical Sciences* **61**, 1059-1064 (2006).

24. Goodpaster BH, Thaete FL, Kelley DE. Thigh adipose tissue distribution is associated with insulin resistance in obesity and in type 2 diabetes mellitus. *Am J Clin Nutr* **71**, 885-892 (2000).

25. Goodpaster BH, Theriault R, Watkins SC, Kelley DE. Intramuscular lipid content is increased in obesity and decreased by weight loss. *Metabolism* **49**, 467-472 (2000).

26. Burakiewicz J, Sinclair CDJ, Fischer D, Walter GA, Kan HE, Hollingsworth KG. Quantifying fat replacement of muscle by quantitative MRI in muscular dystrophy. *Journal of Neurology* **264**, 2053-2067 (2017).

27. Murphy WA, Totty WG, Carroll JE. MRI of normal and pathologic skeletal muscle. *Am J Roentgenol* **146**, 565-574 (1986).

28. Willcocks RJ*, et al.* Multicenter prospective longitudinal study of magnetic resonance biomarkers in a large duchenne muscular dystrophy cohort. *Ann Neurol* **79**, 535-547 (2016).

29. Wokke BH*, et al.* Quantitative MRI and strength measurements in the assessment of muscle quality in Duchenne muscular dystrophy. *Neuromuscular Disorders* **24**, 409-416 (2014).

30. Kopinke D, Norris AM, Mukhopadhyay S. Developmental and regenerative paradigms of cilia regulated hedgehog signaling. *Semin Cell Dev Biol* **110**, 89-103 (2021).

31. Goetz SC, Anderson KV. The primary cilium: a signalling centre during vertebrate development. *Nat Rev Genet* **11**, 331-344 (2010).

32. Hu JK, McGlinn E, Harfe BD, Kardon G, Tabin CJ. Autonomous and nonautonomous roles of Hedgehog signaling in regulating limb muscle formation. *Genes Dev* **26**, 2088-2102 (2012).

33. Anderson C*, et al.* Sonic hedgehog acts cell-autonomously on muscle precursor cells to generate limb muscle diversity. *Genes Dev* **26**, 2103-2117 (2012).

34. Borycki AG, Brunk B, Tajbakhsh S, Buckingham M, Chiang C, Emerson CP, Jr. Sonic hedgehog controls epaxial muscle determination through Myf5 activation. *Development* **126**, 4053-4063 (1999).

35. Pola R*, et al.* Postnatal recapitulation of embryonic hedgehog pathway in response to skeletal muscle ischemia. *Circulation* **108**, 479-485 (2003).

36. Pola R*, et al.* The morphogen Sonic hedgehog is an indirect angiogenic agent upregulating two families of angiogenic growth factors. *Nat Med* **7**, 706-711 (2001).

37. Straface G*, et al.* Sonic hedgehog regulates angiogenesis and myogenesis during post-natal skeletal muscle regeneration. *J Cell Mol Med* **13**, 2424-2435 (2009).

38. Renault MA*, et al.* Desert hedgehog promotes ischemia-induced angiogenesis by ensuring peripheral nerve survival. *Circ Res* **112**, 762-770 (2013).

39. Piccioni A*, et al.* Sonic hedgehog therapy in a mouse model of age-associated impairment of skeletal muscle regeneration. *J Gerontol A Biol Sci Med Sci* **69**, 245-252 (2014).

40. Yao L*, et al.* Gli1 Defines a Subset of Fibro-adipogenic Progenitors that Promote Skeletal Muscle Regeneration With Less Fat Accumulation. *J Bone Miner Res*, (2021).

41. Nosavanh L, Yu DH, Jaehnig EJ, Tong Q, Shen L, Chen MH. Cell-autonomous activation of Hedgehog signaling inhibits brown adipose tissue development. *Proc Natl Acad Sci U S A* **112**, 5069-5074 (2015).

42. Pospisilik JA*, et al.* Drosophila genome-wide obesity screen reveals hedgehog as a determinant of brown versus white adipose cell fate. *Cell* **140**, 148-160 (2010).

43. Palla AR*, et al.* Primary cilia on muscle stem cells are critical to maintain regenerative capacity and are lost during aging. *Nat Commun* **13**, 1439 (2022).

44. Cruz-Migoni SB, Imran KM, Wahid A, Rahman O, Briscoe J, Borycki A-G. A switch in cilia-mediated Hedgehog signaling controls muscle stem cell quiescence and cell cycle progression. *bioRxiv*, 2019.2012.2021.884601 (2019).

45. McKellar DW*, et al.* Large-scale integration of single-cell transcriptomic data captures transitional progenitor states in mouse skeletal muscle regeneration. *Commun Biol* **4**, 1280 (2021).

46. Parmantier E*, et al.* Schwann Cell–Derived Desert Hedgehog Controls the Development of Peripheral Nerve Sheaths. *Neuron* **23**, 713-724 (1999).

47. Caradu C*, et al.* Restoring Endothelial Function by Targeting Desert Hedgehog Downstream of Klf2 Improves Critical Limb Ischemia in Adults. *Circ Res* **123**, 1053-1065 (2018).

48. Brun CE*, et al.* GLI3 regulates muscle stem cell entry into G(Alert) and self-renewal. *Nat Commun* **13**, 3961 (2022).

49. Arjona M*, et al.* Tubastatin A maintains adult skeletal muscle stem cells in a quiescent state ex vivo and improves their engraftment ability in vivo. *Stem Cell Reports* **17**, 82-95 (2022).

50. Bitgood MJ, Shen L, McMahon AP. Sertoli cell signaling by Desert hedgehog regulates the male germline. *Curr Biol* **6**, 298-304 (1996).

51. Mahdy MA, Lei HY, Wakamatsu J, Hosaka YZ, Nishimura T. Comparative study of muscle regeneration following cardiotoxin and glycerol injury. *Ann Anat* **202**, 18-27 (2015).

52. Waisman A, Norris AM, Elías Costa M, Kopinke D. Automatic and unbiased segmentation and quantification of myofibers in skeletal muscle. *Scientific Reports* **11**, 11793 (2021).

53. Lukjanenko L, Brachat S, Pierrel E, Lach-Trifilieff E, Feige JN. Genomic profiling reveals that transient adipogenic activation is a hallmark of mouse models of skeletal muscle regeneration. *PLoS One* **8**, e71084 (2013).

54. Chen X, Li Y. Role of matrix metalloproteinases in skeletal muscle. *Cell Adhesion & Migration* **3**, 337-341 (2009).

55. Senesac CR*, et al.* Magnetic Resonance Imaging Studies in Duchenne Muscular Dystrophy: Linking Findings to the Physical Therapy Clinic. *Physical Therapy* **100**, 2035-2048 (2020).

56. Peverelli L*, et al.* Histologic muscular history in steroid-treated and untreated patients with Duchenne dystrophy. *Neurology* **85**, 1886-1893 (2015).

57. Smith LR, Barton ER. Collagen content does not alter the passive mechanical properties of fibrotic skeletal muscle in mdx mice. *Am J Physiol Cell Physiol* **306**, C889-898 (2014).

58. Agyeman A, Jha BK, Mazumdar T, Houghton JA. Mode and specificity of binding of the small molecule GANT61 to GLI determines inhibition of GLI-DNA binding. *Oncotarget* **5**, 4492-4503 (2014).

59. Zhang R, Wu J, Ferrandon S, Glowacki KJ, Houghton JA. Targeting GLI by GANT61 involves mechanisms dependent on inhibition of both transcription and DNA licensing. *Oncotarget* **7**, 80190-80207 (2016).

60. Aditya S, Rattan A. Vismodegib: A smoothened inhibitor for the treatment of advanced basal cell carcinoma. *Indian Dermatol Online J* **4**, 365-368 (2013).

61. Pisani DF, Bottema CD, Butori C, Dani C, Dechesne CA. Mouse model of skeletal muscle adiposity: a glycerol treatment approach. *Biochem Biophys Res Commun* **396**, 767-773 (2010).

62. Kawai H, Nishino H, Kusaka K, Naruo T, Tamaki Y, Iwasa M. Experimental glycerol myopathy: a histological study. *Acta Neuropathologica* **80**, 192-197 (1990).

63. Gill SE, Parks WC. Metalloproteinases and their inhibitors: regulators of wound healing. *Int J Biochem Cell Biol* **40**, 1334-1347 (2008).

64. Chun TH, Hotary KB, Sabeh F, Saltiel AR, Allen ED, Weiss SJ. A pericellular collagenase directs the 3-dimensional development of white adipose tissue. *Cell* **125**, 577-591 (2006).

65. Jaafar Marican NH, Cruz-Migoni SB, Borycki AG. Asymmetric Distribution of Primary Cilia Allocates Satellite Cells for Self-Renewal. *Stem Cell Reports* **6**, 798-805 (2016).

66. Kopinke D, Roberson EC, Reiter JF. Ciliary Hedgehog Signaling Restricts Injury-Induced Adipogenesis. *Cell* **170**, 340-351 e312 (2017).

67. Fu W, Asp P, Canter B, Dynlacht BD. Primary cilia control hedgehog signaling during muscle differentiation and are deregulated in rhabdomyosarcoma. *Proc Natl Acad Sci U S A* **111**, 9151-9156 (2014).

68. Judson RN, Rossi FMV. Towards stem cell therapies for skeletal muscle repair. *npj Regenerative Medicine* **5**, 10 (2020).

69. CHARGÉ SBP, RUDNICKI MA. Cellular and Molecular Regulation of Muscle Regeneration. *Physiol Rev* **84**, 209-238 (2004).

70. Kang X*, et al.* Interleukin-15 facilitates muscle regeneration through modulation of fibro/adipogenic progenitors. *Cell Commun Signal* **16**, 42 (2018).

71. Vokes SA, Ji H, Wong WH, McMahon AP. A genome-scale analysis of the cis-regulatory circuitry underlying sonic hedgehog-mediated patterning of the mammalian limb. *Genes Dev* **22**, 2651-2663 (2008).

72. Stearns-Reider KM*, et al.* Myoscaffolds reveal laminin scarring is detrimental for stem cell function while sarcospan induces compensatory fibrosis. *bioRxiv*, 2022.2007.2007.497559 (2022).

73. Smith LR, Hammers DW, Sweeney HL, Barton ER. Increased collagen cross-linking is a signature of dystrophin-deficient muscle. *Muscle Nerve* **54**, 71-78 (2016).

74. Kusano KF*, et al.* Sonic hedgehog myocardial gene therapy: tissue repair through transient reconstitution of embryonic signaling. *Nat Med* **11**, 1197-1204 (2005).

75. Piccioni A*, et al.* Sonic hedgehog gene therapy increases the ability of the dystrophic skeletal muscle to regenerate after injury. *Gene Ther* **21**, 413-421 (2014).

76. Kramann R*, et al.* Perivascular Gli1+ progenitors are key contributors to injury-induced organ fibrosis. *Cell Stem Cell* **16**, 51-66 (2015).

77. Hu L, Lin X, Lu H, Chen B, Bai Y. An Overview of Hedgehog Signaling in Fibrosis. *Mol Pharmacol* **87**, 174-182 (2015).

78. Mahdy MAA, Warita K, Hosaka YZ. Early ultrastructural events of skeletal muscle damage following cardiotoxin-induced injury and glycerol-induced injury. *Micron* **91**, 29-40 (2016).